Modeling Seizure Initiation and Spread

Modeling Seizure Initiation and Spread

by
Ling-Ya Monica Chao
Harvard-M.I.T. Division of Health Sciences and Technology

Submitted in partial fulfillment for the degree of
Doctor of Medicine
February 2020

Area of concentration:	Computational neuroscience
Project advisor:	Sydney S. Cash, MD, PhD
Prior degrees:	A.B. (Computer science), A.M. (Physics), MPhil (Computational biology)

I have reviewed this thesis. It represents work done by the author under my guidance/supervision.

Thesis advisor

Acknowledgements

I would like to extend my deepest gratitude to Dr. Sydney Cash, who has been a phenomenal mentor throughout my growth in research, clinical work and life in the past four years. From the beginning, he strongly recommended that I take charge of a new and independent project. Although the learning curve was steep, I gained so much from seeking out my own resources, finding the logical flaws in my arguments, persisting through times when nothing works, and most importantly, being responsible for a piece of scientific work. I am grateful that he gave me this challenge and remained confident in me throughout the process. In addition, his guidance has made the journey doable, extremely rewarding and simultaneously fun and enjoyable. I am always excited to discuss my results with him because he is brilliant at identifying problems in my model design, asking questions that inspire new ideas, suggesting useful resources, and teaching me relevant clinical details. He always sees the big picture and questions it, and intuitively puts our work in the context of its eventual translational potential. His enthusiasm is also contagious; I always leave the meetings feeling excited about our progress and eager to take our work one step further. He has also been deeply committed to my career development and personal growth, helping me navigate the wide array of possibilities at the intersection of clinical medicine and biomedical research. As I will soon embark on a new journey as a neurology resident, I want to again express my sincerest appreciation for Dr. Cash's role in shaping my values and aspirations.

I also want to thank other members of the Cortical Physiology Laboratory at the Massachusetts General Hospital for their endless support, especially to Dr. Louis-Emmanuel Martinet, whose model I built upon in my research and who provided abundant guidance as I learned about various computational models of epilepsy.

Finally, I would like to acknowledge those who have played a significant role in my education. Drs. Rick Mitchell, Matthew Frosch and Junne Kamihara, thank you for your continuous mentorship and support throughout my HST career. Professors Julijana Gjorgjieva, Brandon Westover, Stephen Chong, Jenny Hoffman and Peter Park, thank you for your guidance in research projects that I had previously pursued. And of course, thank you mom, dad, and my fiancé Paul – my tremendously fulfilling experience at Harvard Medical School would not have been possible without you.

Abstract

Epilepsy is a devastating condition, impacting over 50 million people worldwide. Understanding and treating this disease remains a challenge because of its heterogeneous manifestations. A deeper understanding of the underlying biological mechanisms will help pinpoint regions for resection and offer novel targets for pharmacologic or stimulation-based therapies. Here, we present a biophysically and anatomically-motivated model that simulates intracranially-recorded epileptic activity in patients. Our model consists of two components: a mean field model that accounts for the folded geometry of the cortex and electrodes that capture appropriate electrical contributions from neighboring neuronal sources. We also include three elements that were previously proposed to play important roles in seizure dynamics: fast-spiking interneuron population, depolarization block, and evolving extracellular potassium that modulates neural excitability and gap-junction coupling. This model captures several important findings from patient electrographic data of seizures that have been analyzed in previous studies: (1) An ictal wavefront slowly propagates outwards from the epileptogenic focus, recruiting neighboring areas into abnormal activity. Traveling waves emerge within the recruited area and propagate much faster than the ictal wavefront. (2) Contradictory studies proposed that the source of traveling waves is either a stationary cortical source or a moving ictal wavefront. Our model suggests that both cases are plausible and the former happens when the focus is persistent and highly excitable. (3) Seizure terminates spontaneously and synchronously and the frequency of traveling waves decreases before termination. (4) Network coupling increases shortly after seizure onset, decreases during propagation and increases again approaching termination. (5) Consistency of wave direction gradually increases, but the direction can occasionally undergo sudden changes. Overall, the model serves as a means to begin understanding various mechanisms underlying seizure initiation, propagation and termination. It is also greatly customizable and can be adapted to a wide range of unique clinical cases, providing a first step in quick and cost-effective development of personalized therapies.

Contents

List of Figures

Chapter 1

Introduction

Epilepsy is a common neurological disorder characterized by recurrent, unprovoked seizures. Seizures result from excessive and abnormal electrical activity in the brain and can lead to a vast array of clinical presentations, including changes in sensation, loss of awareness, convulsion, memory lapse, etc. But seizures, and epilepsy, are essentially symptoms of other conditions; they can be caused by infections, brain tumors, trauma, stroke and Alzheimer's disease, developmental abnormalities and can often have a genetic basis.

Over 50 million people worldwide suffer from epilepsy; 1 in 26 people will develop it in their lifetime [1]. Fifty to sixty percent of newly diagnosed patients are expected to achieve remission following medical management [2]. The remaining may be considered candidates for a surgical based therapy. Among those that undergo resective surgeries, only 40-50% are free of seizures at 10 years. Accurately localizing the epileptogenic source is often the main challenge in these resections. In addition, surgery is contraindicated for many patients, because of a high risk of damaging areas of the brain responsible for vital functions. Therefore, understanding and treating this devastating condition remains a challenge, not only due to the diverse etiologies but also because of its heterogeneous manifestation in both temporal and spatial domains. Overall, a more accurate prediction of seizure initiation and propagation based on each patient's electrographic activity and brain anatomy can help physicians better pinpoint targets for resection. This would improve the probability of being seizure-free after surgery, reduce complications, and increase the number of candidates for whom resection is suitable. Characterization of ictogenesis and understanding of seizure dynamics will also offer targets for pharmacologic and stimulation-based therapies.

Computational models have gained increased attention in the past few decades as a means to begin exploring the wide variation of seizure dynamics. They are particularly helpful for hypothesizing mechanisms underlying seizure activity prior to designing experiments, and can also serve as a platform for testing interventions *in silico*. Various models have been proposed, each striking a different balance between cellular details and spatial coverage under the limitation of computational power. In this work, we hope to achieve an appropriate middle ground – we present a biophysically and anatomically-motivated model with sufficient spatial scope to allow comparison with patients' intracranial recordings, while including adequate biological details to enable speculation of mechanisms. The model captures several important findings from patient electrographic data of focal seizures that have been analyzed in previous studies (Section 1.2). The model is greatly customizable and can be adapted to a wide range of unique clinical cases, providing a first step in quick and cost-effective development of personalized therapies.

1.1 Computational models of epilepsy

In the past decades, significant advances have been made in electrode technologies. Epileptic activity can now be recorded at different scales, either on the scalp or intracranially. Analysis of these rich data sets have underscored the need for (1) computational models that explain the pathophysiological factors underlying seizure activity; and (2) tools that extract useful clinical information from the observations. This work centers on the first goal but draws from previous research that achieved the second objective.

1.1.1 Network models of the brain

The brain is an extremely complex system, and the challenge faced by any modeling approach is to capture the essential mechanisms while controlling this complexity. The basic building blocks of the nervous system are neurons. By generating action potentials that travel down nerve fibers, neurons relay signals from one part of the body to another. However, to further process the signal and extract useful information, interactions between neurons are essential. Neural circuits are anatomical and functional entities composed of a series of neurons that are connected through chemical and electrical synapses at the end of dendrites and axon terminals. Via these synapses, the activity of one neuron directly influences many others, and the composition of activities enables information flow and processing. To illustrate this framework computationally, networks – nodes connected by edges – are the most commonly used structure. By formulating a mathematical description of the relationship between stimuli and evoked neural responses, computational biologists seek to reproduce neural activity patterns recorded experimentally, which can further aid the understanding of circuit dynamics.

The specific design of neural networks strongly depends on the nature of the data, which can range from single-unit recordings, to recordings of small populations of neurons as is found in local field potential (LFP) signals, to recordings that summarize activity of large neuronal populations at lower spatial resolution, like electroencephalographic (EEG) signals. Accordingly, models at all levels of details have been proposed to explain epileptic activity; a node in the network can represent a single neuron, a population of neurons of the same type or even multiple populations. Broadly speaking, existing models for seizures can be categorized into three groups, in decreasing order of cellular details and increasing order of spatial coverage (see Figure 1.1 for schematic illustrations) [3]:

- *Detailed network models*: Each node consists of either a principal neuron or an interneuron and edges represent synapses and/or gap junctions between two neurons [4]. Details like neuron morphology and ion channels are often included to investigate the impact of cellular abnormalities (e.g. channelopathies). Data sets are usually local field potential (LFP) signals, which capture the electric potential in the extracellular space around neurons and can be acquired through microelectrode arrays like NeuroPort.
- *Neural mass models* (NMMs, or neuronal population models): Each node summarizes the average activity (e.g. firing rate) and properties (e.g. resting potential) of a population of a specific type of neuron; explicit cellular details are often kept to the minimal [5, 6]. Interactions between nodes reflect the amount of chemical and electrical coupling between different cell types. Similar to detailed network models, NMMs are usually developed in conjunction with LFP recordings. Note that NMMs cannot be used to analyze spatial dynamics

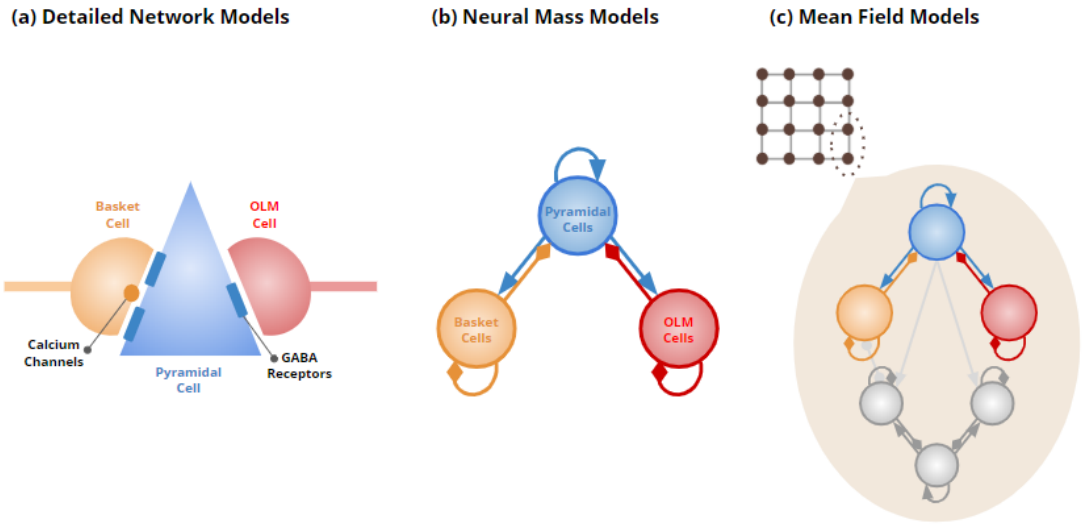

Figure 1.1: **Schematic illustrations of the three categories of network models.** (a) In detailed network models, each node is a neuron and edges represent chemical or electrical connections between neurons. (b) In neural mass models, each node represents a population of neurons and edges are the global interactions between different populations. (c) In mean field models, each node is a neural mass model with localized dynamics, and edges represent longer-range interactions.

---

because activity of all neurons of the same type is averaged.

- *Mean field models* (MFMs): To capture the both the spatial and temporal evolution of neural activity, mean field models couple together multiple NMMs [7, 8, 9, 10]. More specifically, each node in the network is a NMM, with its own subpopulations and local dynamics, and the nodes can interact with each other through long range connections like myelinated axons. This type of model enables the study of spatiotemporal patterns, including traveling waves, at the scale of specific cortical regions or even the entire brain. It is most commonly used to reproduce electroencephalogram (EEG) recordings, obtained either on the scalp or intracranially. Intracranial EEG (iEEG) includes both depth EEG, which is recorded through thin wires within the depth of the brain, and electrocorticography (ECoG), where a grid of electrodes are placed directly on the cortical surface.

Besides these categories of biologically-inspired models, mathematical (or phenomenological) models have also been developed to study seizure dynamics [11]. They usually do not link specific equations to neurological mechanisms, but instead focus on how the formulations enable evolving, abstract variables to exhibit behaviors similar to that of real-life recordings. Although more remote from clinical applications, they have the advantage of covering all possible cases and can be studied analytically. They were not considered for this work because we intend to propose novel therapies for epilepsy and the underlying mechanisms are of high relevance.

Among biophysical models, a mean field model is utilized here because we are interested in reproducing interesting spatiotemporal patterns observed in intracranial electrographic data from epilepsy patients. However, we also draw from detailed network models and include some cellular properties like ion conductance, because abundant research has suggested that alterations in ion concentration are strongly linked to seizure dynamics. Overall, our model could

be considered an extended mean field model, with emphasis on anatomical scope while not losing sight of important biophysical elements that have direct clinical implications.

1.1.2 Mean field models of epilepsy

Among all three categories of seizure models, mean field models are arguably the least researched (although they are used more often in other capacities, e.g. sleep and anesthesiology research). One potential reason is that many simplifications need to be made to make models at such large spatial scale run in a reasonable amount of time. Assumptions are also necessary because we not yet have experimental data with sufficient coverage. Both of which make reproducing clinical data much more challenging. For example, since the network connectivity and neural density of the human brain have not been characterized in full, MFMs usually assume that these parameters are homogenous across the cortex, which is not accurate and can lead to failure to capture some interesting spatial fluctuation.

One of the most recent MFMs for seizure is proposed by Cosandier-Rimele et al. and it models the relationship between the activation of brain sources and the corresponding depth EEG and scalp EEG signals [9]. Although it also briefly describes neuronal dynamics within the cortex, it focuses mainly on how electrical activity is registered by electrodes. Another model that exhibits the nature of a MFM is the Epileptor neural field model [12]. It is, however, generally considered a mathematical model instead of a biophysical one. Each network node is represented by five different variables, which jointly represent three interacting time scales. Spatially, the model is one dimensional and does not include anatomical information, but it reproduces many qualitative findings on seizure spread and termination. Lastly, Martinet et al. also proposed a MFM, specifically to address the underlying mechanism of increased spatial coupling towards the end of a seizure (see Section 1.2.2 for more details) [8]. Our work builds upon his model, with the aim of capturing additional spatiotemporal features observed in human seizure data.

1.1.3 Perspectives of computational models

Computational models have implications in both neuroscience research and clinical epileptology. They aggregate large amount of data in a logical manner, and help scientists understand neural dynamics based on neurophysiological hypotheses, which can then be tested experimentally. In scenarios where experimental assessments are difficult, models provide a means for testing hypotheses *in silico*. Clinically, models of epileptic activity can be useful for physicians facing convoluted and variable situations: they reduce the complexity of the mechanism and emphasize the underlying physiology. Pharmacologically, such understanding aids in the development of targeting medications. Tailored surgery on the genesis and propagation of seizures in a patient-specific context is another fascinating perspective of modeling.

Computational models are often criticized for being overly simplified, sacrificing biological realism or imposing unrealistic assumptions. However, it is noteworthy that the aim of creating theoretical models is often to temporarily remove the complexity and intertwinement of biological details and unveil the minimal mechanism required to explain observed phenomena [13]. When a proposed scheme fails to explain the experimental data, more features can be included and the necessity of them can be examined or proven along the way. On the other hand, if a model is

successful, biological details can also be added and the researchers will have a clearer idea of how to avoid disturbance to the existing system. Overall, it is useful to start with a simple model as long as it encompasses flexibility for future modification and re-evaluation.

1.2 Experimental background

Understanding the spatiotemporal dynamics of seizure and the biological mechanisms governing them is an extremely difficult task, both because of the limited spatial resolution of recording technologies as well as the heterogeneity intra- and inter-patients. However, dynamics at several time scales have been observed in patient data and modeled computationally: (1) ictogenesis, the transition from the interictal state to seizure – in a focal seizure, there is usually an onset zone where seizure is initiated; (2) propagation of seizure from recruited areas to non-recruited areas (slow traveling ictal wavefront); (3) emergence of low amplitude, fast oscillations (> 10 Hz) in recently recruited areas; (4) transition into spike-and-wave complexes or burst-suppression patterns towards seizure termination, and (5) synchronized seizure termination. This section will cover several findings related to these dynamics. At the end, we also briefly discuss the long debated topic of spatial coupling during the ictal period. Many of these findings are reproduced in our model, and our hope is that it will shine some light on the widely discussed field.

1.2.1 Ictogenesis and ictal wavefront propagation

Current understanding of acquired epilepsy suggests that an insult (e.g. brain tumor, hypoxic injury) leads to reorganization of the brain, which can include neuronal loss, gliosis (reactive change of glial cells), alterations in membrane channels/receptors of neurons, etc. These changes make the brain more prone to seizures. However, they do not fully explain the process of ictogenesis, which specifically refers to the acute process of seizure generation by an epileptogenic brain. The biological mechanisms underlying ictogenesis has yet to be fully understood, and similar to the mechanisms underlying propagation and termination, may vary between different epileptic syndromes. Potential mechanisms that have been proposed include: (1) a shift in the reversal potential of GABA-mediated currents, resulting in excitation from GABAergic input; (2) exhaustion of presynaptic GABA release; (3) synchronization of many neurons by interneurons [14, 15, 16, 17, 18]. In this work, we will propose an alternative explanation of ictogenesis that primarily depends on the slow accumulation of extracellular potassium, which has been proposed to play an important role in seizure propagation (as described in the next few paragraphs).

After focal seizures initiate in a localized region of the brain, it slowly spreads to a larger cortical area. Mechanistically, areas that are recruited into the seizing zone exhibit high excitatory activity, which directly or indirectly changes the excitatory and inhibitory balance in connected areas (which are usually but not always neighboring) and leads to propagation of seizure into those areas. The moving edge of the seizing zone is termed the ictal wavefront and the speed is usually on the order of 1 mm/s [12, 19]. It is important to note that, standard clinical EEG interpretation techniques usually cannot detect the ictal wavefront. This could possibly be due to its limited spatial extent, which results in obscuration by spatial averaging of electrodes, or due to its lack of sufficient temporal organization that produces detectable oscillations [20]. Evidence of ictal wavefront can instead be detected with microelectrodes, though the ability to evaluate its spatial extent is limited by the spatial span of the electrodes.

How the ictal wavefront propagates and what determines its velocity are widely debated. Classically, breakdown or weakening of a surrounding inhibitory barricade is thought to enable spreading of seizure activity. Several *in vitro* studies have shown that strong inhibition around the onset focus can suppress the excessive excitatory drive, preventing local pyramidal cells from being excited and seizure from spreading [21, 22]. If propagation does begin, inhibitory activity can also control the spread dynamics: Trevelyan et al. found that the higher the number of preictal inhibitory barrages, the slower the propagation velocity, and that velocities can vary over a 1000-fold range [21]. The main contributor to this "feed-forward inhibition" is thought to be parvalbumin-expressing fast-spiking interneurons, which are consistently observed to have increased firing rate prior to interictal-ictal transition in some models of seizure activity [23, 24, 25, 26, 27]. Although the number of these interneurons are much lower than pyramidal neurons, they synapse directly on the nearby pyramidal cell bodies at high concentration and thus provide strong inhibitory power, counteracting the excitatory currents originating from the seizing areas. Electrographically, this surround inhibition has been described as the ictal "penumbra", where local field potentials exhibit heterogeneous activity (representing pyramidal activity mixed with inhibitory activity vetoing it) but the region has yet to be recruited to seizure.

Various mechanisms have been hypothesized to lead to failure of this inhibitory restraint, allowing runaway excitation and spreading of seizure. The majority of these mechanisms were observed in animal models. The precise role of them in human seizures is still unclear, though the increasing amount of human multi-unit and single-unit data recently has allowed more studies targeting this topic. To date, evidence has pointed to interneuron depolarization bock and altered chloride homeostasis as two possible etiologies of failed inhibitory restraint.

With regards to the theory of depolarization block, Cammarota et al. utilized Ca^{2+} imaging to show that the parvalbumin-expressing fast-spiking interneurons experience a firing impairment caused by membrane depolarization preceding ictal onset of neighboring pyramidal cells. Other studies have also shown that seizure-like events terminate when inhibitory neurons resume activity, which further supports the connection between depolarization block and the seizing state [27]. To the best of our knowledge, the causal relationship between depolarization block and ictal wavefront propagation is less clear in human *in vivo* recordings. Ahmed et al. examined firing rate tracings of nearby fast-spiking interneurons and regular-spiking excitatory neurons from seizing patients [28]. Instead of sequential activation described above, both populations start firing simultaneously, in contrast to the hypothesis that cessation of fast-spiking cells precedes and directly leads to seizure propagation. However, in alignment with *in vitro* data, the authors also observed that the fast-spiking cells cease firing half-way through a seizure and local seizure amplitude increases at the same time, thus it is still likely that their inhibitory effect plays a role in altering seizure dynamics.

The mechanism of fast-spiking interneurons entering depolarization block continues to be widely debated. It is hypothesized that extracellular potassium can play a role. Pathological elevation of extracellular potassium level (to as high as 12-15 mM) is seen during seizures with both *in vivo* and *in vitro* experiments [29, 30, 31, 32]. Theoretically, this elevation shifts the reversal potential of potassium towards zero and increases the excitability of various populations of neurons (both excitatory and inhibitory). However, with excessive depolarization, selected populations are prone to go into depolarization block. To explore the effect of this change computationally, Ahmed et al. developed a single-cell, Hodgkin-Huxley model [28]. Different from the normal excitatory cells, they modeled fast-spiking interneurons

with a larger potassium conductance. This is based on prior patch clamp studies, which showed increasing amount of Kv3.1 channels on fast-spiking cells [33, 34, 35]. After this feature was added, the authors simulated a progressively increasing extracellular potassium concentration, as observed during seizures. Interestingly, the fast-spiking cells exhibit features seen in single-cell recordings from seizing patients: their firing rate increases initially, then quickly ceases midway through the seizure.

To briefly discuss the dynamics of elevating extracellular potassium, it is important to mention the Potassium Accumulation Hypothesis, initially proposed by Fertziger and Ranck in 1970 [32]. The core idea is that a transient increase in potassium over a certain threshold can trigger a positive feedback loop: neurons become more depolarized with elevated extracellular potassium, fire more action potentials and release more potassium into the extracellular space. Glial cells normally serve as a spatial buffer to prevent excessive accumulation of extracellular potassium and maintain homeostasis of brain excitability. Specifically, locally elevated potassium drives its influx into glial cells, which is then distributed via intercellular gap junctions to a distal location where potassium level is low. Glial tissue also has the ability to store potassium and temporarily relieve any excess. In events of glial dysfunction (e.g. scarring), this clearance mechanism could be impaired, tilting the excitatory-inhibitory balance of nearby tissue [36].

It is important to point out that, as described above, the observed potassium elevation drives the reversal potential of potassium towards zero and increases excitability of various neural populations. In addition to driving interneurons into depolarization block, it also causes excitatory populations to be hyperactive. This duality raises the question of whether the excitatory population's hyperactivity alone is sufficient to overcome the inhibitory barrier and enable seizure propagation, or if breakdown of the inhibitory barrier is necessary.

To conclude this section, we discuss an alternative mechanism for the weakening of inhibitory restraint – dysregulation of chloride homeostasis. This hypothesis first stemmed from studies of neonatal seizures. It was observed that, in the neonatal period, high expression of NKCC1 and low expression of KCC2 make neurons more susceptible to intracellular chloride accumulation, which in turn leads to GABA having paradoxical excitatory effect and facilitating neonatal seizures [37]. Similar alterations in KCC2 and NKCC1 expressions are also seen in adult brain gliomas, which are known to be highly epileptogenic [38]. It is hypothesized that, during a seizure, intense feedforward activation from the already-recruited area leads to increased intracellular chloride concentration in the pyramidal cells, compromising (or even reversing) GABA-dependent inhibition from interneurons and contributing to seizure propagation. However, recent studies have suggested that this mechanism alone is not sufficient to trigger a seizure. Optogenetically loading pyramidal cells (on mouse neocortical slices) with chloride does not induce ictal events without adjunct pathology (in the same study, the adjunct pathology was done with bathing model in 4-aminopyridine, a selective blocker for the delayed rectifier type potassium channels) [39]. Overall, it is likely that multiple mechanisms jointly enable spreading of ictal-like events.

1.2.2 Spike-and-wave complexes and traveling waves

Once recruited into the seizing zone, neural populations continue to show evolving spatiotemporal dynamics. Low amplitude, fast oscillations ($>$ 10 Hz) emerge first and later on, large amplitude spike-and-wave complexes (SWCs, 2-3 Hz) are seen. In this work, we will focus on the latter as it is better understood and modeled.

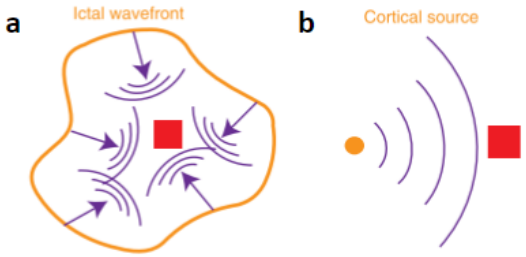

Figure 1.2: **Two theories for source of traveling waves.** Adapted from [8]. (a) The expanding ictal wavefront (orange) produces traveling waves (purple) that are registered by the electrodes (red). Proposed in [40], based on data analysis that shows opposite directions of ictal wavefront and traveling waves. (b) A fixed cortical source produces traveling waves (purple) that are registered by the electrodes (red). Supported in [8], as their analysis showed high consistency of traveling wave directions, more suggestive of a fixed source.

Martinet et al. examined the SWCs in voltage tracings from microelectrode arrays (spacing of 0.4 mm) and macroelectrode arrays (i.e. electrocorticogram, spacing of 1 cm) implanted in three patients [8]. They showed that coupling (assessed via coherence, a frequency-domain measure of linear association) between these spatial scales increases towards seizure termination and decreases with distance between electrodes. To further characterize the spatial organization of this coupling, the authors analyzed the delay between electrodes and suggested that the increase in inter-scale coupling during later stages of seizure results from spike-and-wave complexes emerging and propagating through the field. The estimated speed of these "traveling waves" is between 100 to 1000 mm/s, orders of magnitudes faster than the recruiting ictal wavefront. In addition, the direction estimates of these waves become more consistent over time and are similar between seizures in the same patient and across spatial scales, supporting the source of traveling waves being a fixed cortical location – the ictal core (demonstrated in Figure 1.2b). The authors concluded with a computational model capturing the observed seizure dynamics. The model includes an evolving extracellular potassium concentration that modulates neural excitability. Elevated potassium is also hypothesized (and modeled accordingly) to close gap junctions between inhibitory populations via slow acidification of the extracellular environment and in turn support the emergence of inter-scale coupling. The model presented in this work is an extension of Martinet et al.'s computational framework (see Chapter 2 for more details) and will further explore the role of potassium in both ictal wavefront propagation and traveling waves [8].

It is important to note that, another study by Smith et al. reported contradicting results on the source of traveling waves [40]. They identified that the directions of the waves and the propagating ictal wavefront are opposite, which led them to hypothesize that the source is moving and consists of the slow ictal wavefront itself (demonstrated in Figure 1.2a). Both scenarios suggest that seizure terminates when the source of traveling waves dissipates; however, in the fixed cortical source model, termination requires failure of a small ictal core, while in the moving wavefront model, termination involves weakening of the entire ictal wavefront. It is possible that both scenarios can occur, especially in a heterogeneous patient cohort. Part of this work will identify network parameters and underlying biological mechanisms that determine which scenario dominates.

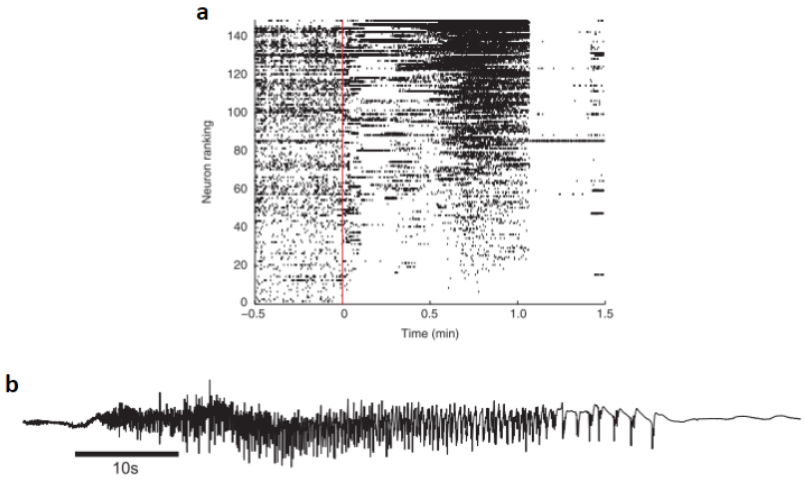

Figure 1.3: **Characteristics of seizure termination.** (a) Adapted from [42]. A neuronal spike raster during seizure in human subject, showing simultaneous cessation of spiking activity at seizure termination. (b) Adapted from [51]. An example voltage tracing from ECoG electrode spanning an entire seizure. Increasing inter-spike spacing prior to seizure termination is often referred as "brain chirp".

1.2.3 Seizure termination

Mechanisms driving seizure termination remain one of least understood topics in epilepsy. However, (macroscopic) electrographic recordings of seizures from patients usually exhibit some stereotypical dynamics prior to transition to the post-ictal period. Specifically, there is a characteristic slowing of rhythmic activity (often described as "brain chirp", see Figure 1.3b, an example voltage tracing from a single ECoG electrode during seizure) and increasing coupling (as described in the previous section), followed by sudden and synchronous cessation of activity cross the recorded field (Figure 1.3a, an example spike raster recorded *in vivo* during seizure) [41, 42, 43]. This progression has been studied and modeled in various capacities. Kramer et al. identified the dynamics as a critical transition between two stable states (attractor states) and reproduced it with a mean field model that exhibit bistability [41]. The same model could also reproduce status epilepticus dynamics, which was hypothesized to represent repeated approaches to the critical transition without actually crossing it. Interestingly, some of the signatures of critical transition (specifically, the "flickering" phenomenon, where noise pushes a bistable system between two states) was not observed at the scale of the microelectrode array, suggesting that seizure termination could be a macroscopic phenomenon, necessitating collective interaction of neural populations across a larger area.

A more mechanistic model for seizure termination was proposed by Smith et al., who, as described in the previous section, hypothesized that the ictal wavefront is the source of traveling waves [40]. They designed a mean field model that suggested that weakening of the ictal wavefront (modeled manually as reduced external input) is sufficient to reproduce the slowing of rhythmic discharges and eventual cessation, though the underlying mechanism remains to be determined. Studies in animal models have suggested various biophysical explanations, including depletion of energy source (e.g. adenosine triphosphate) or neurotransmitters (e.g. glutamate), change in ion gradients across membrane, decreased pH and modulatory effects from subcortical structures, etc [44, 45, 46, 47, 48, 49, 50]. Unfortunately, testing

these hypotheses have been very challenging in humans.

1.2.4 Coupling and network organization

One of the most widely debated topic in epilepsy is the role of synchronization, or coupling, between different brain areas. Historically, seizures were thought to be a state of hyper-synchrony, where increased connectivity in the seizure focus leads to excessive activity. With advancement of recording technologies, the organization and coupling of activity are now recognized to evolve during different phases of seizure (onset, propagation, termination and interictal period). However, there is no consensus on how the coupling actually changes during each period - analyses have yielded widely varying results, possibly due to differences in coupling measures, type of seizures, electrode type and placement, definition of seizure phases, etc.

An excellent review on the spatio-temporal evolution of network organization was written by Kramer [51]. Here, we highlight some of the important content and hypotheses proposed in his review with regards to coupling during various phases of seizure:

- *Onset*: In the higher frequency bands, decoupling has been observed between different gyri and during beta frequency discharges from patients with mesial temporal lobe epilepsy [52, 53]. It is also observed in depth and strip electrode recordings from patients with complex-partial and secondarily generalized seizures [54]. This can possibly be interpreted as functional disconnection between distant brain regions when seizure initiates locally at the focus. Interestingly, when examining lower frequency bands (< 30 Hz), increased correlation was seen immediately after seizure onset [55]. This may be a reflection of the gradual recruitment of cortex into seizure activity.
- *Propagation*: Similarly, there is also lack of consensus regarding the degree of coupling during seizure propagation. Linear correlation appears to decrease upon transition from seizure onset to propagation, while non-linear measures (e.g. synchronization likelihood, phase coherence) continues to suggest increased coupling [55, 56, 57]. One proposed theory for decreased coupling during propagation hypothesized that excessive neuronal firing at seizure onset saturates "hub neurons", which maintain local connectivity. When these neurons enter refractory periods, a functional disconnection ensues.
- *Approaching termination*: Most studies have agreed on the observation that coupling of brain activity increases approaching seizure termination. This is seen with both linear and non-linear measures, as well as across seizure types [55, 58, 54]. In particular, synchrony reaches maximal value during the last part of a seizure. As mentioned in the previous section, Martinet et al. hypothesized that this increase is a result of emergence of traveling waves. An alternative proposal suggested that a self-organization of neuronal activity aiming to drive the hyperactive neurons into refractory state could be the source of the increased coupling [59].

1.3 Thesis overview

In this thesis, I present an *in silico*, network-based, biophysically-motivated representation of realistic seizure activity in the human brain. It reproduces several experimental findings described above and provides new insights

into the diagnosis and treatment of epilepsy.

The outline is as follows:

- In Chapter 2, I introduce the mean field model and describe all the mathematical formulations and model parameters. For each design choice, I will either link it to an existing experimental finding or propose biophysical mechanisms that support it.
- In Chapter 3, I will present a sample simulation and show how the simulated electrical readings match various qualitative and quantitative behaviors of patient recordings. How model parameters influence simulation outcome and their physiological/medical implications are also discussed.
- In Chapter 4, I summarize the main findings in this thesis and highlight the novelty and contribution of the model. I also discuss the limitations of the current model and suggest several refinements and prospective directions of exploration.

Chapter 2

Model Framework and Analytical Tools

I developed an anatomically-motivated model that simulates intracranially-recorded epileptic activity in patients. It is characterized as a biophysical framework because each variable is associated with a biophysical entity and every formulation represents a known or hypothesized mechanism. The model consists of two parts that jointly simulate electrographic recordings: (1) a network-based, cortical mean field model (MFM) that includes an epileptogenic focus; (2) simulated electrodes that capture appropriate electrical contributions from neighboring neuronal sources and generate recordings that can be compared to patient data. In this chapter, we will present these two components in detail and discuss several analytical tools we use to characterize the simulated recordings and facilitate the comparison between our model and known experimental findings.

2.1 Mean field model

To represent both the spatial and temporal evolution of neural activity, we adapt a mean field model. Many mean-field formulations exist [9, 10], and here we choose to extend an existing two-dimensional MFM, developed by Martinet et al. [8], which is itself an adaption of a framework by Steyn-Ross et al., previously applied to simulate sleep, cognitive states and anesthesia [7]. As described later in this chapter, we modify the model in ref [8] by transforming the grid-like network into a geometrical brain surface and adding several elements that were previously proposed to play important roles in seizure dynamics.

In the MFMs proposed by Martinet et al. and Steyn-Ross et al., the cortex is represented as a two-dimensional grid of nodes (either or 100×100, 120×120) in square formation, corresponding to approximately 300 mm by 300 mm cortical surface. Each node represents superimposed populations of excitatory and inhibitory neurons within approximately 9 mm^2. Each population is characterized by its average neural activity (average soma potential and average firing rate). This omits the variability of activity between individual neurons, but since electrodes can only sense average voltages generated by population of neurons, the model's ability to capture electrographic data is not compromised. Nodes are interconnected locally via gap junctions and over long distances via myelinated axons.

To represent the temporal and spatial dynamics mathematically, the soma excitatory and inhibitory potentials

V_e and V_i at grid location $\vec{r} = (x, y)$ obey the following differential equations (adapted from [7]):

$$\begin{aligned}\tau_b \frac{\partial V_b(\vec{r},t)}{\partial t} &= V_b^{\text{rest}} + \Delta V_b^{\text{rest}} - V_b(\vec{r},t) \\ &+ [\rho_e \psi_{eb}(\vec{r},t)\Phi_{eb}(\vec{r},t) + \rho_i \psi_{ib}(\vec{r},t)\Phi_{ib}(\vec{r},t)] \\ &+ D_b \nabla^2 V_b(\vec{r},t) \end{aligned} \tag{2.1}$$

where b is either e or i, representing excitatory or inhibitory populations respectively. Symbols with two subscripts ab adopt a left-to-right convention with presynaptic population $a = \{e, i\}$ and postsynaptic population $b = \{e, i\}$. $\nabla^2 = \partial^2/\partial x^2 + \partial^2/\partial y^2$ is the standard 2D-Laplacian operator. The terms in square brackets represent synaptic inputs, while the final term represents contributions from gap-junction currents between nearby neurons. More specifically, each parameter is defined as following:

- τ_b are time constants for the neuron populations, representing how fast a neuron reaches it target value.
- V_b^{rest} are resting potentials for each population. ΔV_b^{rest} are the offsets to the resting potentials, representing the excitability of neurons. In simulations where a seizure is manually incited, this value is set to a positive number around the seizure focus.
- ρ_b are strengths of synaptic connections, approximated with the area under the excitatory and inhibitory postsynaptic action potential. By definition, $\rho_e > 0$ and $\rho_i < 0$. These strengths are scaled by reversal potential functions

  $$\psi_{ab} = \frac{V_a^{\text{rev}} - V_b(\vec{r},t)}{V_a^{\text{rev}} - V_b^{\text{rest}}} \tag{2.2}$$

  which has a value of 1 at resting potential and approaches 0 when soma voltage reaches the reversal potentials ($V_e^{\text{rev}} = 0$ mV and $V_i^{\text{rev}} = -70$ mV).
- The $\Phi_{ab}(\vec{r},t)$ functions represent synaptic fluxes, which are derived from the following differential equations. For simplicity, only excitatory neurons emit long-range flux in this model.

  $$\left(\frac{\partial}{\partial t} + \gamma_e\right)^2 \Phi_{eb}(\vec{r},t) = \gamma_e^2 [N_{eb}^{\alpha} \phi_{eb}^{\alpha}(\vec{r},t) + N_{eb}^{\beta} Q_e^{\beta}(\vec{r},t) + \phi_{eb}^{sc}(\vec{r},t)] \tag{2.3}$$

  $$\left(\frac{\partial}{\partial t} + \gamma_i\right)^2 \Phi_{ib}(\vec{r},t) = \gamma_i^2 N_{ib}^{\beta} Q_i(\vec{r},t) \tag{2.4}$$

  - γ_b are rate constants, assuming that the reaction of postsynaptic neuron in response to dendritic input obeys an alpha-function with form $\gamma^2 t e^{-\gamma t}$.
  - The superscripts α and β denote long-range and local connections respectively. N_{ab}^{α} and N_{ab}^{β} are the number of each type of connection.
  - $Q_b(\vec{r},t)$ are local fluxes directly proportional to local firing rate, which is approximated as a sigmoidal function of the soma voltage:

    $$Q_b(\vec{r},t) = \frac{Q_b^{\max}}{1 + \exp[-\frac{\pi}{\sqrt{3}} \frac{V_b(\vec{r},t) - \theta_b}{\sigma_b}]} \tag{2.5}$$

    where θ_b is the average threshold for firing, σ_b is the standard deviation, and $Q_b^{\max}$ is the maximum firing rate.

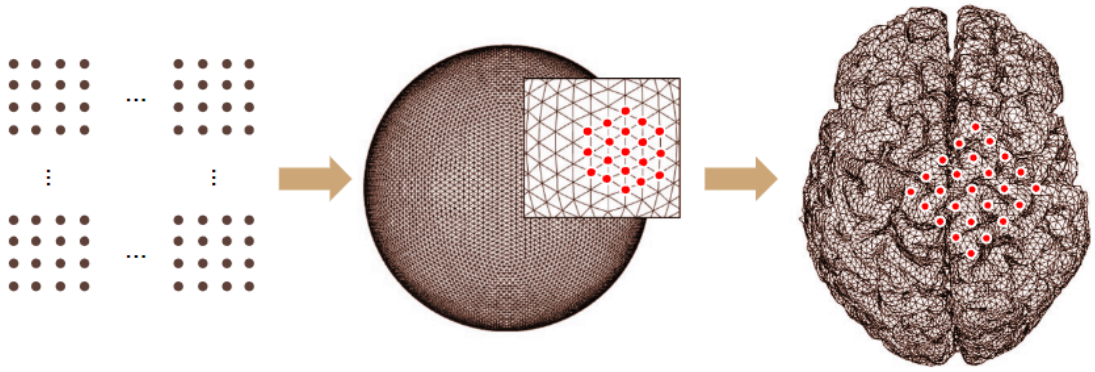

Figure 2.1: **Stepwise updates in model complexity.** We first extend the existing two-dimensional model to a triangular mesh of the sphere, consisting of 10242 nodes. Electrodes are modeled by recording the activity at selected nodes (represented by red dots). For higher spatial resolution and anatomical accuracy, we further increase the number of nodes to 40962 and morph its shape to match a sample cortical geometry. Electrodes are modeled by overlaying a 5x5 grid on the area of interest and averaging the activity of nearby nodes, weighted by reciprocal distances.

– ϕ^{α}_{eb} are fluxes through long-range connections, modeled as damped waves generated by distant excitatory neurons, obeying the following equation:

$$\left[\left(\frac{\partial}{\partial t}+v\Lambda_{eb}\right)^2-v^2\nabla^2\right]\phi^{\alpha}_{eb}(\vec{r},t)=(v\Lambda_{eb})^2Q_e(\vec{r},t) \tag{2.6}$$

where Λ_{eb} is the inverse-length scale for axons of excitatory neurons and v is the axonal conduction speed.

– ϕ^{sc}_{eb} represents input from subcortical sources, modeled as white noise around a constant background $\langle\phi^{\text{sc}}_{eb}\rangle$:

$$\phi^{\text{sc}}_{eb}(\vec{r},t)=\langle\phi^{\text{sc}}_{eb}\rangle+a\sqrt{\langle\phi^{\text{sc}}_{eb}\rangle}\xi_{eb}(\vec{r},t) \tag{2.7}$$

where a is a amplitude scaling factor and ξ_{eb} is a randomized function that obeys Gaussian distribution.

- D_b are the coupling strength between neuron pairs connected via gap junctions. We assume that gap junctions are only present between neurons of the same type (excitatory-excitatory or inhibitory-inhibitory). In addition, as there are many more gap junctions between inhibitory neurons than excitatory neurons, it is assumed that $D_e = D_i/100$ for easier computing [60] and D_i has a minimum value of 0.1.

In the rest of the chapter, we describe various modifications and additions we incorporate into the above base model:

To begin to understand how seizure activity manifests on the brain surface, we need to design a model that accounts for the complex cortical geometry. We first simplify the problem by modeling the cortex as a sphere. Instead of using a square grid in the papers described above, our network is configured as a triangular mesh on the sphere consisting of 10242 nodes, each connected with six immediate neighbors via weighted edges. The radius of the sphere is 10 cm and average distance between neighboring nodes is 0.378 cm. See the middle image in Figure 2.1 for an example of the network.

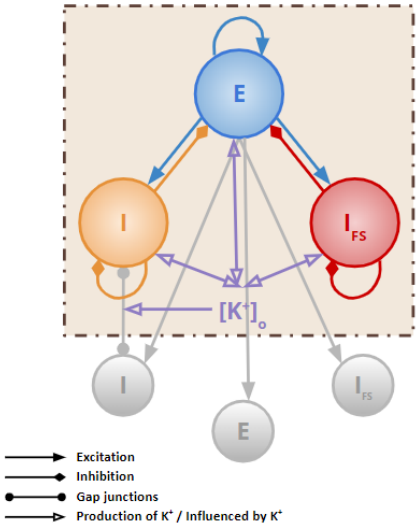

Figure 2.2: **Cartoon illustration of the model.** The dotted rectangle represents one node in the triangular mesh. In each node, one excitatory (E) and two inhibitory (I_{FS} for fast-spiking interneurons and I for other inhibitory neurons) neural populations interact with each other through synapses as well as with spatial neighbors (grayed-out circles) through gap junctions and synapses. Activity of each cell population increases the local extracellular potassium concentration, which diffuses in space and elevates the resting potential of nearby populations.

After various biophysical modifications are incorporated to adequately capture several qualitative and quantitative behaviors of patient recordings, we then aim for higher spatial resolution and anatomical accuracy. This is achieved via increasing the number of nodes to 40962 (keeping the radius at 10 cm, and now average distance between neighboring nodes is 0.189 cm) and warping the sphere into the geometry of a cortex. The triangular mesh of the cortical surface is acquired through *FreeSurfer*. This progression of anatomical complexity is portrayed in the right most image of Figure 2.1. We assume that the density of neurons and the connectivity between populations are constant across the entire cortex. This is a significant simplification of the human brain's heterogenous network, but the model is designed with great flexibility and customizability to include connectome data when available.

In addition to the geometrical adaptations, we also include several biophysical elements that were previously known to play important roles in seizure dynamics (cartoon illustration of the model in Figure 2.2). The most important addition is fast-spiking (FS) interneurons. As described in Section 1.2.1, mice models have suggested that ictal wavefront propagation (i.e., recruitment of cortex into seizure activity) is possibly dependent on failure of inhibitory restraint in the setting of FS interneurons entering depolarization block. It is hypothesized that these cells are more susceptible to depolarization block due to an alteration in potassium conductance, thus they more readily enter depolarization block as extracellular potassium level increases. To incorporate this into our model, we add a third neuron population (in addition to the existing excitatory and inhibitory populations) to each node. They are also inhibitory in nature and depress postsynaptic activity. The subscript used for this population is f, so Q_f for local firing rate of FS interneurons, N_{fe} for number of synapses from FS interneurons to excitatory neurons, etc. For simplicity, we do not connect neighboring FS interneurons with gap junctions. To account for the inhibitory input

from these FS interneurons to local excitatory population, we update Equation 2.1 for the excitatory soma potential to:

$$\begin{aligned}\tau_e \frac{\partial V_e(\vec{r},t)}{\partial t} &= V_e^{\text{rest}} + \Delta V_e^{\text{rest}} - V_e(\vec{r},t) \\ &+ [\rho_e \psi_{ee}(\vec{r},t)\Phi_{ee}(\vec{r},t) + \rho_i \psi_{ie}(\vec{r},t)\Phi_{ie}(\vec{r},t) + \rho_f \psi_{fe}(\vec{r},t)\Phi_{fe}(\vec{r},t)] \\ &+ D_e \nabla^2 V_e(\vec{r},t) \end{aligned} \tag{2.8}$$

where Φ_{fe} obeys

$$\left(\frac{\partial}{\partial t} + \gamma_f\right)^2 \Phi_{fb}(\vec{r},t) = \gamma_f^2 N_{fb}^{\beta} Q_f(\vec{r},t) \tag{2.9}$$

and for simplicity, we assume: $\rho_f = \rho_i$, $\gamma_f = \gamma_i$, and ψ_{fe} and $Q_f(\vec{r},t)$ obey the same equations as the non-FS inhibitory neurons.

To model potassium dynamics and its effects, we follow Martinet et al. and include a slowly evolving variable representing the changing concentration of extracellular potassium, which is known to increase dramatically during seizure and other abnormal brain conditions. Potassium interacts with the existing variables in several ways. First, activity of neurons increase the local concentration of potassium, which subsequently diffuses in space or gets reabsorbed by glial cells. Similar to the regular-spiking excitatory and inhibitory populations, the FS interneurons also produce potassium into the extracellular space. However, as their membrane has higher conductivity to potassium, we hypothesize that they produce potassium at a rate faster than other populations and model this accordingly. Specifically, the extracellular potassium concentration K obeys the following equation:

$$\tau_K \frac{\partial K}{\partial t} = -C_1 K + \frac{C_2 Q_{\text{total}}}{1 + e^{-(Q_{\text{total}} - \delta)}} + C_3 \nabla^2 K \tag{2.10}$$

τ_K is the time constant for potassium dynamics. The first term represents a decay of K at rate C_1 via reabsorption. As described in Section 1.2.1, in normal tissue, glial cells serve as spatial buffer to prevent excessive accumulation of extracellular potassium. To capture this in our model, we designate two zones on the geometrical surface: one where glial function is impaired (pathological zone, small C_1) and the rest where potassium homeostasis is adequately maintained (normal zone, large C_1). The second term describes potassium efflux from excitatory and inhibitory neurons during activity. It is modeled as a sigmoid function scaled by rate C_2 and threshold of δ. $Q_{\text{total}} = Q_f + c(Q_e + Q_i)$ and $c < 1$ is a scaling factor representing relative contribution of non-FS vs FS neurons. The last term represents diffusion of potassium to neighboring locations, at a rate of C_3. Of note, elevation of K is limited to a ceiling value of 12, which was determined from electrically and pharmacologically induced activity in cat cortex [61].

The extracellular potassium K acts to decrease the gap junctions between inhibitory neuron populations (of note, as described above, the strength of gap junctions between excitatory populations continue to obey $D_e = D_i/100$):

$$\frac{\partial D_i}{\partial t} = -\frac{K}{\tau_D} \tag{2.11}$$

where τ_D is the time constant for this perturbation. In general, this time constant is set at the order of seconds to minutes so that these variables change slowly.

In order to capture the influence of potassium conductance and intra- and extracellular potassium concentration on resting membrane potential (and in turn, excitability and activity) of each population, we incorporate the Goldman-

Hodgkin-Katz (GHK) voltage equation:

$$V_b^{\text{rest}} = \frac{RT}{F} ln \left(\frac{p_{K,b}[K^+]_o + p_{Na}[Na^+]_o + p_{Cl}[Cl^-]_i}{p_{K,b}[K^+]_{i,b} + p_{Na}[Na^+]_i + p_{Cl}[Cl^-]_o} \right) \tag{2.12}$$

where $p_{x,b}$ is the conductance for ion $x = \{K, Na, Cl\}$ for population $b = \{e, i, f\}$. We abbreviate $p_{Na,b} = p_{Na}$ and $p_{Cl,b} = p_{Cl}$ as we assume the conductance for sodium and chloride are approximately the same between different neuron types. To represent increasing potassium conductance in FS interneurons, we set $p_{K,f} = \epsilon p_{K,e} = \epsilon p_{K,i}$ where $\epsilon > 1$. $[x]_{i,b}$ is the concentration of ion x in the intracellular space for population $b = \{e, i, f\}$. $[x]_o$ is the concentration in extracellular space ($[K^+]_o = K$ as defined above). Similar to conductance, we abbreviate $[Na^+]_{i,b} = [Na^+]_i$ and $[Cl^-]_{i,b} = [Cl^-]_i$ as we assume the intracellular concentration for sodium and chloride are approximately the same between different neuron types. We also assume that $[K^+]_{i,e}$ and $[K^+]_{i,i}$ are constant, as regular-spiking excitatory and inhibitory neurons produce potassium at a much slower rate so potassium homeostasis can likely keep the intracellular concentration stable. On the other hand, since we hypothesize that the FS interneurons output potassium much faster, we model $[K^+]_{i,f} = [K^+]_{i,f}^{\text{init}} - \upsilon([K^+]_o - [K^+]_o^{\text{init}})$ such that the intracellular concentration proportionally (rate υ) decreases as extracellular concentration increases.

Lastly, to enable depolarization block, we follow Martinet et al. and designate the firing rate of each population to approach zero when greatly depolarized (membrane voltage less negative). To achieve this, a Gaussian activation function instead of the sigmoid function described above (Equation 2.5) is applied to convert soma voltage to local firing rate:

$$Q_b(\vec{r}, t) = \frac{Q_b^{\max}}{1 + \exp[-\frac{\pi}{\sqrt{3}} \frac{V_b(\vec{r},t) - \theta_b}{\sigma_b}]} - \frac{Q_b^{\max}}{1 + \exp[-\frac{\pi}{\sqrt{3}} \frac{V_b(\vec{r},t) - \theta_b'}{\sigma_b'}]} \tag{2.13}$$

where θ_b' is the average threshold for depolarization block, σ_b' is the standard deviation. Of note, Martinet et al. did not find a role for the depolarization block in generating the low-frequency dynamics simulated in their paper. However, as detailed in the following chapters, it has significant importance in the simulation of the ictal wavefront in this project.

Simulation of spontaneous ictogenesis is still a work in progress in our project. For the majority of the simulations and results presented in Chapter 3, we incorporate a manually-incited seizure focus, where we increase excitability in a cluster of nodes (i.e. set $\Delta V_b^{\text{rest}} = 8$ within these nodes). However, in the last section of Chapter 3, we present some preliminary data on an advanced model with spontaneous ictogenesis. We also discuss some existing limitations of this model, and we are are hopeful that, with further work, these limitations can be solved.

The standard values of the above parameters are listed in Table 2.1. The model is written in MATLAB. Simulation is performed step-wise at a time scale of 0.002 seconds, with most runs lasting a total of 300 seconds (thus $300 \div 0.002 = 150,000$ steps in total). Data is sampled and recorded every 0.02 seconds (i.e. 10 steps) for further analysis. On average, to simulate a 300-second event, the model with 10242 nodes takes 50 minutes and one with 40962 nodes takes approximately 180 minutes.

Symbol	Value	Unit	Description
$\tau_{e,i,f}$	0.04, 0.04, 0.04	s	neuron time constant
$\Delta V_{e,i,f}^{\text{rest}}$		mV	offset to resting potential
$\rho_{e,i,f}$	10^{-3}, -1.05×10^{-3}, -1.05×10^{-3}	mV s	excitatory and inhibitory synaptic gain
$V_{e,i,f}^{\text{rev}} = 0$	0, -75, -75	mV	reversal potential at the dendrite
$\gamma_{e,i,f}$	170, 50, 50	1/s	excitatory and inhibitory rate constant
$N_{ee,ei,ef}^{\alpha}$	2000, 2000, 666	-	long-range cortico-cortical axonal connectivity
$N_{ee,ei,ef}^{\beta}$	800, 800, 266	-	local axonal connectivity from excitatory population
$N_{ie,ii}^{\beta}$	670, 600	-	local axonal connectivity from inhibitory population
$N_{fe,ff}^{\beta}$	5, 20	-	local axonal connectivity from FS inhibitory population
$Q_{e,i,f}^{\max}$	30, 60, 40	1/s	maximum firing rate
$\theta_{e,i,f}$	-58.5, -58.5, -58.5	mV	average threshold for firing
$\sigma_{e,i,f}$	3, 5, 5	mV	standard deviation for firing threshold
$\theta'_{e,i,f}$	-40.5, -40.5, -40.5	mV	average threshold for depolarization block
$\sigma'_{e,i,f}$	1, 1.66, 1	mV	standard deviation for depolarization block
$\Lambda_{ee,ei,ef}$	4, 4, 4	1/cm	inverse length scale for axons of excitatory population
v	280	cm/s	axonal conduction speed
a	4	-	subcortical noise scaling factor
$\langle \phi_{ee,ei,ef}^{\text{sc}} \rangle$	300, 300, 100	1/s	average subcortical input
D_i	0.1 (initial value)	cm^2	gap junction strength between inhibitory populations
D_e	D_i / 100	-	gap junction strength between excitatory populations
D_f	0	-	gap junction strength between FS inhibitory populations
τ_K	200	s	time constant for K dynamics
C_1, C_2, C_3	0.05, 10, 1	-, mM s, cm^2	scale factors for various contributors to extracellular K (reabsroption, production, diffusion)
δ	3	1/s	threshold for production of K during neural activity
c	0.1	-	relative contribution of non-FS vs FS neurons to extracellular K
τ_D	133	mV s / cm^2	time constant for perturbation of gap junction strength
ϵ	1.3		conductance for K in FS neurons (relative to normal-spiking)
p_{Na}, p_{Cl}	0.04, 0.45		conductance for sodium and chloride (relative to potassium)
υ	18		rate of intracellular K deviation relative to extracellular deviation

Table 2.1: List of parameters used in the model and choices for their values.

2.2 Simulated electrodes

To facilitate comparison between our computational model and electrographic recordings from epilepsy patients, we also simulate electrodes that capture electrical activity within the mean field model described above. Since recordings from patients are performed at different scales (10-by-10 microelectrode array with electrode spacing of 0.4 mm and 8-by-8 macroelectrode array with electrode spacing of 10 mm), we also model electrodes at of various spatial span.

In the reduced sphere framework (10242 nodes), electrodes are modeled by simply recording the activity at selected nodes that spatially resemble two concentric hexagons (total 19 electrodes). Example shown as red dots in the middle image of Figure 2.1. We adapt a hexagonal geometry instead of a grid like structure because it more appropriately lines up with the triangular mesh. Macroelectrode and microelectrode are both modeled in this manner with different spatial span, with the former 4 times the size of the latter.

In the more realistic, anatomical framework, we model electrodes by identifying a 5x5 grid that overlays the cortical area of interest (red dots in the right image of Figure 2.1). More technically, we first identify the desired location of the center of the grid (somewhere in the pathological zone, small distance away from the designated seizure initiation site), then compute the vector perpendicular to the brain surface at that location. Lastly, we identify the plane perpendicular to this vector and tangential to the brain surface, and place the grid on this plane. Again, there are two types of electrodes with different spatial scale. For the macroelectrode array, the distance between electrodes is 9 mm, so size of the entire array is 36 x 36 mm. For the microelectrode array, the distance between electrodes is 0.5 mm, so size of the entire array is 2 x 2 mm. Each electrode summarizes activity of nearby network nodes, weighted by their reciprocal distances, i.e. the closer the node is to the electrode, the more it contributes to its recording.

2.3 Analytical tools

As described in Section 1.2.4, characterizing synchronicity (or coupling) between different areas of the brain is a key component to understanding dynamics of seizures. Following Martinet et al.'s work in [8], we also assess coupling via calculation of coherence. Figure 2.3 is reproduced from the same paper and shows an example pipeline for analyzing a seizure recording from patient. We adapt it to analyze simulated recordings from our model. Specifically, we estimate the time-dependent coherence between the recorded activity of two electrodes using the Chronux Toolbox. We divide the data into 10-second windows with 9-second overlap and compute the frequency-dependent coherence within each window using a time-bandwidth product of 20 and 39 tapers (Figure 2.3a is an example coherogram between two random electrodes from patient data). To summarize the coherence across the frequency spectrum, we compute the average coherence between 1 and 13 Hz (Figure 2.3b). This frequency interval is chosen as the highest coherence in human seizure data is observed within this range (as represented with the red areas in Figure 2.3a). Furthermore, because coherence between two electrodes varies with distance between them, in order to assess how the overall coupling evolves throughout a seizure, we also need to define one variable ("global coherence") that summarizes the coherence between every pair of electrodes over a certain period of time. Here, we perform linear regression of coherence versus inter-electrode distance and extract the left-intercept as the global coherence. An example is shown in Figure 2.3c, which shows coherence versus electrode distance for a single seizure recording from patient. For each time interval (pre-seizure, early seizure, middle seizure, late seizure), a linear regression is performed. We can see that, although the left-intercept does not fully capture the distribution of data, it appears to be a good surrogate for comparison of relative degree of coupling between different time periods.

In order to study the emergence of traveling waves, we employ another analytical tool that seeks to identify traveling waves from electrode recordings and compute the velocity of these waves. First, we identify the "delay" between each pair of electrodes. We follow the approach in [62] and [8] and utilize the phase of the coherence.

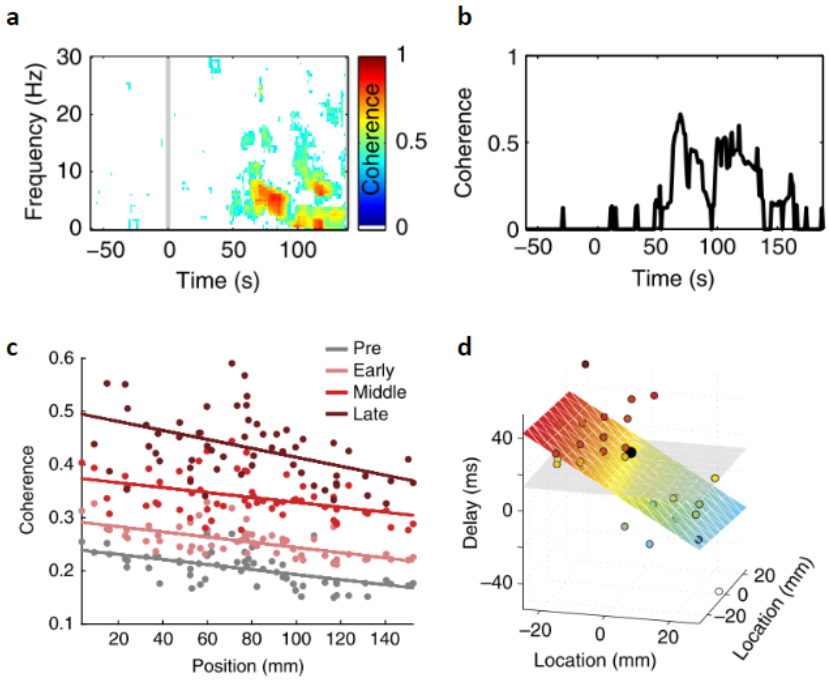

Figure 2.3: **Example of various analytical tool applied to human recordings.** Reproduced from [8]. (a) Coherogram between two random electrodes. (b) Average coherence between the same two electrodes in (a) within frequency range 1 and 13 Hz versus time. (c) Coherence versus electrode distance at different periods of a seizure. The left intercept is what we define as the "global coherence" for a specific period. (d) We compute traveling wave source direction and velocity (at a specific time point) by performing linear regression of delays between electrodes as a function of their relative location.

Specifically, we identify an interval of 3 Hz (within 1-13 Hz as described above) or larger with consecutive significant coherence. Within this interval, we perform a linear fit of phase (of the coherence) versus frequency. If the fit is significantly better than a constant term model, the slope provides an estimate of delay between two electrodes. If the fit is poor, the delay is considered undefined. To identify traveling waves within the spatial span of an electrode array (either microelectrodes or macroelectrodes), we incorporate the analysis in [8]. We perform a linear regression of the delays between each electrode and the central electrode $\mathbf{D}$ as a function of their relative location $(\mathbf{X}, \mathbf{Y})$ to the central electrode, $\mathbf{D} = b_0 + b_1\mathbf{X} + b_2\mathbf{Y}$ (Figure 2.3d is an example from patient data). For a fit to be considered valid, at least 50% of the electrodes for that window have a defined delay and the fit model needs to be significantly better than constant term model. Once a valid fit is identified, the wave speed is computed as $\frac{1}{\sqrt{b_1^2+b_2^2}}$ and direction of the wave is estimated as the arctan $\left(\frac{b_2}{b_1}\right)$.

Chapter 3

Simulation Examples and Analysis Results

Given the large parameter space of our model, the simulation result varies widely depending on choice of combination of parameters. Many could be physiological and reflect the heterogeneity of patient cohort, while some are much less likely to be a good representation of human data. To maintain sufficient validity of our model, we frequently revisit various analyses of human recordings to ensure that our model can reproduce some key qualitative and quantitative features. In this chapter, we first present a typical simulation from the spherical model and discuss these specific features. For features where the underlying physiological mechanism is still widely debated, we attempt to contribute to the discussion by proposing distinct models that could possibly reflect each scenario. In the second section of this chapter, we present the cortical model, which has higher spatial resolution and anatomical accuracy, and show that the same features from human recordings can be reproduced as well. Last, we present some preliminary data from our attempt to simulate the spontaneous occurrence of ictogenesis.

3.1 Spherical model

Figure 3.1 shows a simulation of the model with a spherical network of 10242 nodes. Here, the epileptogenic focus is manually incited ($\Delta V_b^{\text{rest}} = 8$ in a cluster of 7 nodes) for 10 seconds (our preliminary result for simulating ictogenesis without a manual external input is described in Section 3.3). Only the activity of the hemisphere centering on the epileptogenic focus is shown: blue nodes represent populations that are quiescent and yellow nodes suggest high excitatory population activity. The pink dots are location of the macroelectrodes (microelectrodes are not plotted).

Neural dynamics are observed at two different time scales.

As described in Section 1.2, neural dynamics are observed at two different time scales in patient recordings. When seizure initiates in a localized epileptogenic focus, an ictal wavefront slowly propagates to recruit areas into abnormal activity. Later in the seizure, traveling waves (spike-and-wave discharges) are recorded instead. These waves are estimated to propagate orders of magnitude faster than the ictal wavefront (100-1000 mm/s versus 1 mm/s). This two-fold dynamics is accurately captured in our model.

Firstly, if we consider the ictal wavefront as the outer circumference of the area with abnormal activity, we can see that in the first 150 seconds of simulation, the wavefront is propagating outwards away from the epileptogenic center. The area that it "sweeps" subsequently begins to exhibit increased firing rate, matching experimental results.

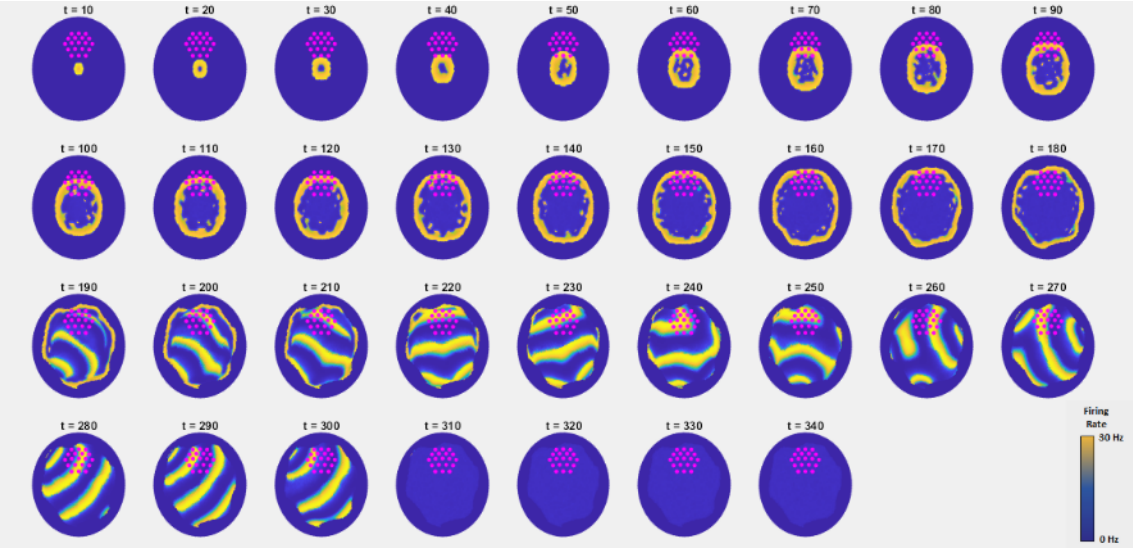

Figure 3.1: **Example spatial maps of simulated activity.** Each subfigure shows a snapshot (time t labeled above each) of the excitatory population activity. Only the hemisphere centered around the focus is shown here. When seizure initiates in a localized epileptogenic focus, a wavefront slowly propagates outwards, recruiting neighboring areas into high-frequency activity. Later in the course, traveling waves emerge from the wavefront and propagate through the recruited area. Seizure eventually terminates spontaneously and synchronously. The simulated macroelectrodes are indicated as pink dots.

In our model, the wavefront expands at a speed approximately 0.7 mm/s, comparable to human experimental data (estimated at 1 mm/s) [8, 12]. This suggests that the mechanism we included in our model (fast-spiking interneurons and its susceptibility to enter depolarization block, as defined in Chapter 2) can possibly explain the propagation of ictal wavefront. Specifically, during seizure propagation, the ictal wavefront generates feed-forward input to the neighboring unrecruited area and excites the local inhibitory populations there. These inhibitory populations provide restraint that opposes epileptiform spread while contributing to extracellular potassium accumulation through positive feedback. The FS interneurons have the strongest interaction with extracellular potassium: their rapid firing contribute the most to $[K^+]_o$ and their resting potential is consequently elevated the most due to higher membrane permeability to potassium and faster loss of intracellular potassium. This positive feedback dynamics makes them more susceptible to depolarization block. When FS interneurons reach depolarization block, inhibition breaks down and the area (or node in the network) is recruited into seizure.

Complementary to the global scale dynamics, we also attempt to use this model to explore single-neuron dynamics. As described in Section 1.2.1, the causal relationship between depolarization block and seizure propagation is less definitive in human single-neuron recordings. Specifically, Ahmed et al. observed that, around the preictal-ictal transition, pyramidal cells and nearby FS interneurons are activated simultaneously instead of sequentially (as what would be expected from the mechanism described in the previous paragraph). We hope to possibly reconcile this discrepancy with our model. In Figure 3.2, we show the simulated activity of the FS interneurons and excitatory neurons at a randomly chosen electrode. Notably, FS inhibitory activity increases quickly as the seizure spreads. There is some simultaneous excitatory activity, but the amplitude is small as it is limited by the interneurons. Soon after, FS interneuron activity suddenly ceases due to depolarization block; this transition is accompanied by a

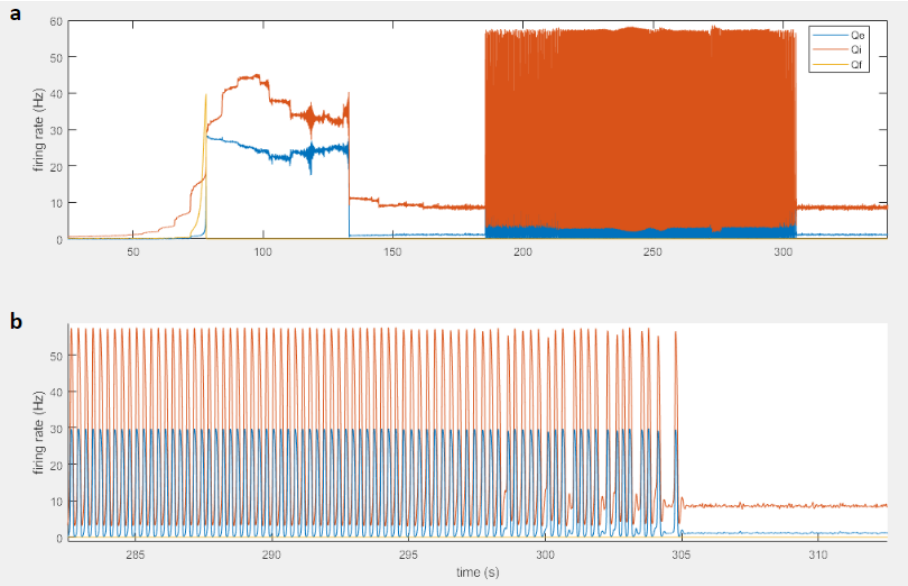

Figure 3.2: **Firing rate of each population at a randomly chosen electrode.** (1) Entire seizure course. Notably, FS cells (yellow tracing) cease firing midway through a seizure due to depolarization block and local excitatory activity (blue tracing) dramatically increases. (2) Zoomed in to the time period around seizure termination. Notably, rhythmic activity slows down prior to complete cessation.

---

dramatic increase in local excitatory activity. With these tracings, we wonder if the discrepancy above could stem from differences in the definition of seizure recruitment and ictal onset. At the peak of the feedforward inhibition, there could already be some excitatory activity (via feedforward excitation from areas already exhibiting ictal activity), albeit moderately suppressed by interneurons. Whether this activity is considered as ictal could potentially influence the interpretation of the causal relationship between depolarization block and seizure recruitment.

Here, we would also like to propose an alternative mechanism for ictal wavefront propagation. Similar to how elevated extracellular potassium can drive FS interneurons into depolarization block, it also causes excitatory populations to be hyper-excitable. To understand if this hyperactivity alone is sufficient to trigger seizure propagation, we experimented with a model without FS interneurons (in our model, this is equivalent to setting $Q_f^{max} = 0$ and $N_{fe}^{\beta} = 0$). After exploring the parameter space, we were able to reproduce very similar dynamics (Figure 3.3). However, to achieve physiological speed for ictal wavefront propagation, the potassium production rate of the normal-spiking excitatory and inhibitory neurons needs to be high to trigger a sufficiently fast positive feedback of potassium accumulation. This is certainly possible, especially in patients with channelopathies, and could be suggestive of distinct mechanisms of seizure propagation in different disease pathologies.

In addition to physiologic ictal wavefront propagation, our model reproduces the traveling waves as well. Seconds after an area is recruited into the seizing zone, large amplitude spike-and-wave complexes (SWCs, 2-3 Hz) emerge and propagate, forming traveling waves. The velocity of these waves is approximately 350 mm/s, which is orders of magnitudes faster than the recruiting ictal wavefront, consistent with observations from human recordings. In our model, we adapt the mechanism proposed by Martinet et al. to achieve this transition – specifically, increasing local

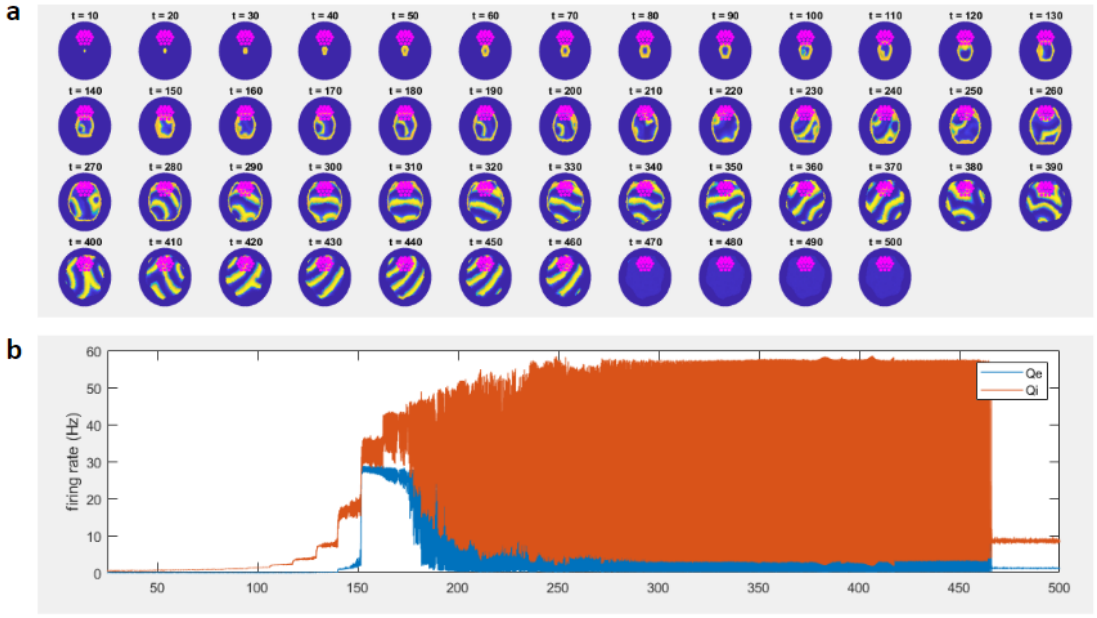

Figure 3.3: **Simulation of seizure course with model that does not have a fast-spiking interneuron population.** (a) Spatial maps at various time points. (b) Activity of excitatory and inhibitory (regular-spiking) populations. Dynamics of ictal wavefront propagation and traveling waves are again reproduced, suggesting that hyperactivity of pyramidal cells in setting of elevated extracellular potassium could be sufficient to explain seizure propagation.

---

extracellular potassium weakens the gap junction strength between inhibitory populations and allows Hopf (temporal) instability to drive large-scale oscillations and traveling waves. This is just one of the possible underlying mechanisms for emergence of traveling waves, but it nicely ties into the ion dynamics (specifically potassium) suspected to contribute to ictal wavefront propagation.

Source of traveling waves can be either a stationary cortical source or a moving ictal wavefront

Studies have presented contradicting data that support the source of traveling waves as being either a stationary cortical source or a moving ictal wavefront. Martinet et al. showed that the direction estimates of these waves become more consistent over time and are similar between seizures in the same patient and across spatial scales, supporting the source of traveling waves being a fixed cortical location – the ictal core [8]. In contrast, Smith et al. identified that the directions of the waves and the propagating ictal wavefront are opposite, which led them to hypothesize that the source is moving and consists of the slow ictal wavefront itself [40].

Our model suggests that both cases are plausible, especially in a heterogeneous patient cohort. If the focus is transient, the ictal wavefront constitutes a stronger source and produces the traveling waves recorded by electrodes (as seen in Figure 3.1). On the other hand, if the focus is highly excitable throughout most of the seizure duration, either due to persistent cortical abnormalities or sustained subcortical input, the epileptogenic focus is very active and serves as a stationary wave source. To model this, we manually assign $\Delta V_e^{\text{rest}} = 8$ to the epileptogenic focus for

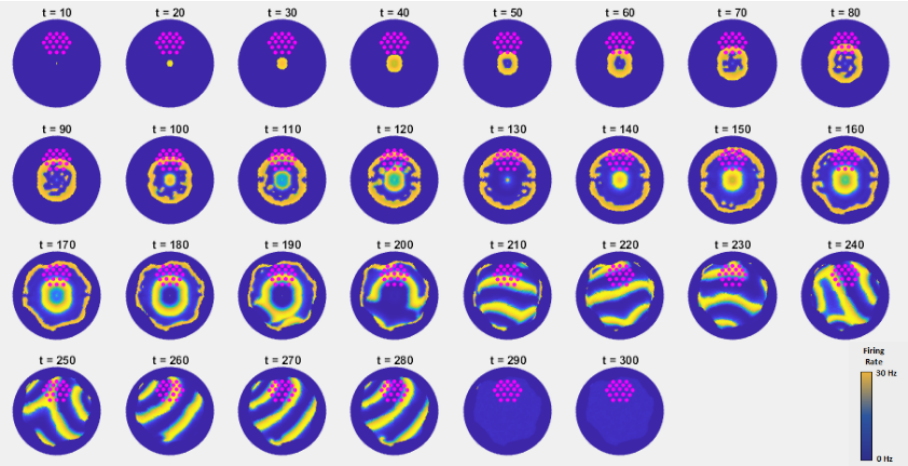

Figure 3.4: **Seizure course with highly excitable and persistent epileptogenic focus.** In this case, the focus serves as the stationary wave source when active, different from the simulation in Figure 3.1, where the ictal wavefront serves as the traveling wave source.

---

200 seconds to indicate persistent excitability. Simulation results are shown in Figure 3.4, which demonstrate that, when the focus is still active, it continuously emits traveling waves that can be captured by the electrodes.

Coupling within the cortical network increases shortly after seizure onset, decreases during propagation and increases again approaching termination.

Next, we address the controversial topic of cortical network coupling. As discussed in Section 1.2.4, although it is generally known that synchronicity of network activity is a feature that distinguishes epileptic cortex from normal brain, there is not yet a comprehensive and consistent characterization of the cortical organization throughout different phases of seizure. We contribute to this conversation by assessing the temporal evolution of coupling in our model, using coherence between pairs of electrodes as surrogate. To enable comparison of coherence across time points, we define a "global coherence", which is the left intercept when performing linear regression of coherence versus inter-electrode distance (see Section 2.3 for details). Figure 3.5 shows how this value changes as seizure progresses. We note that multiple simulations with either identical or different model parameters show consistent trend in coherence: it increases shortly after seizure onset, decreases during propagation and increases again approaching termination. Although readings from both macroelectrodes and microelectrodes show this trend, it is more apparent at the microscopic scale. By aligning the evolution of coherence with visualized spatial activity at different time points, we hypothesize that the supporting mechanism is as follows: (1) At seizure onset, coherence increases as the ictal wavefront propagates across the electrode grid to sequentially recruit populations (nodes) into abnormal activity. (2) Shortly after recruitment into the seizure zone, gap junction strength between inhibitory populations is still high. Waves emerge from the ictal wavefront and other seizing areas that have high activity, but the waves are very weak, do not travel far and collide with other waves soon after emergence. This results in a chaotic dynamics and hence the decrease in coherence. (3) As potassium accumulates and gap junction weakens, waves can travel over long distances without inhibition. As a result, the populations with the highest activity (either the ictal wavefront or epileptogenic focus, as discussed earlier in this section) dominates and serves as the source for traveling waves. The propagation of

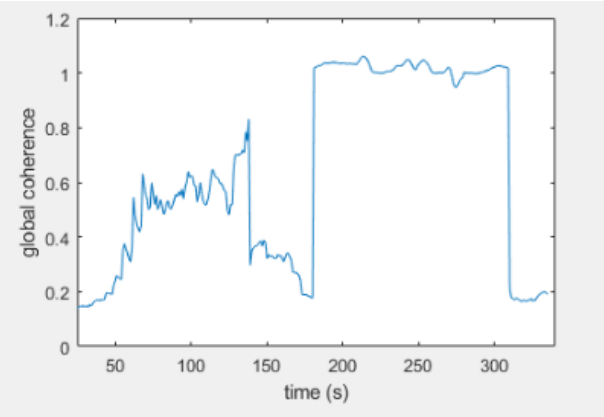

Figure 3.5: **Coherence analysis.** Global coherence (see text for definition) at the microelectrodes over time. The general trend of this value is consistent across simulations with varied parameters: it increases at onset, decreases during propagation and increases again approaching termination.

---

these waves couples population activity over large cortical areas and supports the increase of coherence approaching seizure termination.

Consistency of wave source direction increases later in the seizure, but the direction can occasionally undergo sudden changes.

To quantitatively characterize the spatial organization of the traveling waves and compare it with human seizure data, we examine the evolution of the estimated source direction at the center of the simulated microscopic and macroscopic electrodes. Briefly, to compute this, we calculate the delay between each electrode and the central electrode and estimate the traveling wave direction and velocity by performing multiple linear regression of the delay over the spatial distribution of the electrode grid (see Section 2.3 for more details). Figure 3.6a shows the evolution of estimated source direction corresponding to the simulation presented in Figure 3.1. Direction at time points where the linear fit is poor is not shown as it indicates a lack of detectable traveling waves at the electrode location. We note that the consistency of source directions increases throughout the seizure at the microscopic and macroscopic spatial scales, coherent with results from statistical analyses of human seizure data [8]. This applies to both scenarios where the wave source is either a moving ictal wavefront or a stationary focus. Interestingly, in simulations where the ictal wavefront initiates traveling waves, analysis reveals sudden changes in source direction several times throughout the seizure. This phenomenon is previously observed in microelectrode array data from seizure patients (Figure 3.6b shows wave source analysis of recordings from three patient data, reproduced from [8]) and, to the best of our knowledge, has not been captured in other computational models [63]. Mechanistically, our model suggests that the spatial heterogeneity of the ictal wavefront governs the changes in direction. Different parts of the ictal wavefront exhibit different levels of activity and the segment with the highest activity dominates and serves as the source of traveling waves. As seizure progresses, the ictal wavefront propagates outward from the focus and eventually interacts with pathological and structural boundaries, resulting in continuous changes in the relative strength of different parts of the wavefront. As a result, the source direction changes from time to time.

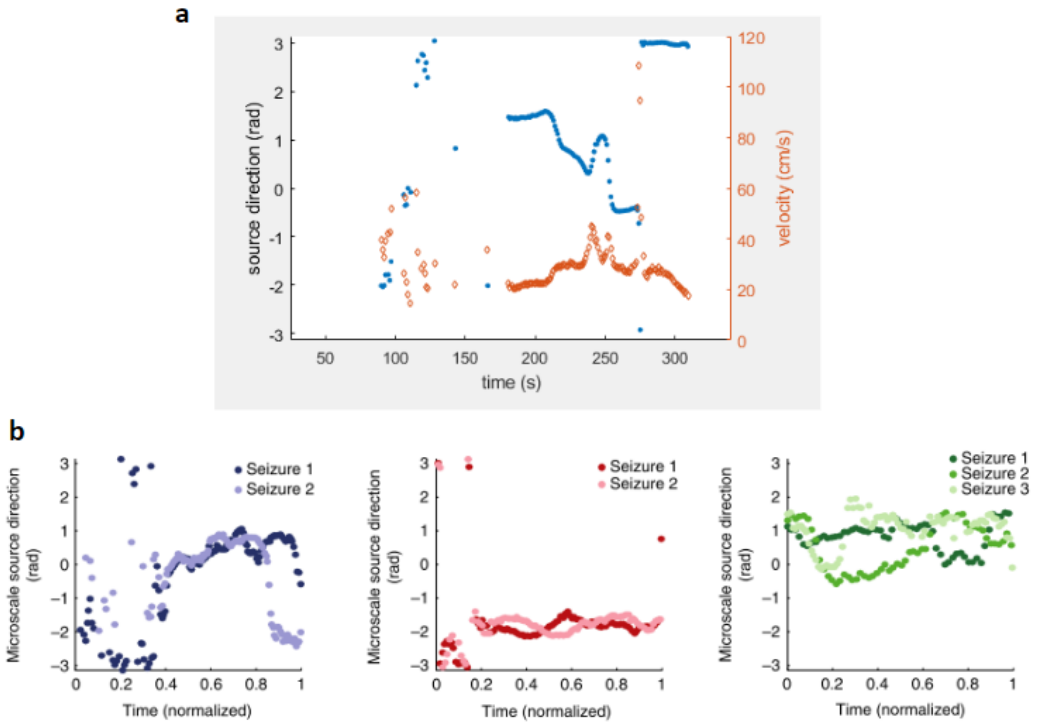

Figure 3.6: **Traveling wave analysis.** (a) The source direction and velocity recorded at the microelectrodes over time. Direction at time points when the linear fit is poor is not shown. Consistency of source direction increases towards seizure termination but direction occasionally undergo sudden changes. (b) Traveling wave source direction analysis of microelectrode recordings from three patients, reproduced from [8].

Seizure terminates spontaneously and synchronously and the frequency of traveling waves decreases before termination.

As discussed in Section 1.2.3, one characteristic electrographic finding of seizure termination is the slowing of rhythmic activity ("brain chirp") followed by synchronous cessation of activity across the entire seizing field, irrespective of the temporal delay in recruitment. Here, we propose possible supporting mechanism for this dynamics specifically in the scenario where the ictal wavefront serves as the source of traveling waves. We hypothesize that there is a different mechanism that supports termination in the scenario with a stationary cortical source, e.g. adaptive inhibitory input from subcortical sources.

As shown in Figure 3.1, our model successfully captures the spontaneity and synchronicity of seizure termination. Without varying any global parameter midway through the simulation, abnormal activity ceases spontaneously when the ictal wavefront reaches the boundary of the pathological zone. Outside of the pathological zone, potassium homeostasis is normal and fast-spiking neurons do not enter depolarization block from potassium accumulation. Consequently, the ictal wavefront fails to recruit more areas into seizure and it gradually weakens when confronted with strong inhibition from the normal brain regions. Since the wavefront serves as the source for traveling waves, when it dies out, the waves cease and activity stops in the entire recruited zone nearly synchronously. Note that this

does not imply that the pathological zone has returned to normal physiological stage. In our model, potassium is still elevated within and the zone is still excitable, but there is not a strong source that generates longer range activity. To the best of our knowledge, this mechanism of seizure termination has not been proposed previously. Our model suggests that it is theoretically a possible scenario for synchonized termination of seizure, and further experiments can be designed to prove or disprove this hypothesis.

Of note, in addition to the spontaneous and synchronous termination of seizure, the model also reproduces the slowing of rhythmic activity prior to termination. Figure 3.2b shows the firing rate of various populations prior to seizure termination (i.e. a zoomed in version of 3.2a) and suggests that the frequency of spikes-and-waves decreases prior to complete cessation. Figure 3.6a also shows that the velocity of traveling waves decreases prior to termination. This matches very well with the "brain chirp" phenomenon. Mechanistically, this slowing is likely due to weakening of the ictal wavefront, which as a consequence, leads to weakening of the traveling waves.

We observe that the spontaneous termination of seizure can depend on a wide variety factors. Interestingly, decreasing the global long-range inhibition N_{ie}^{b} by even 0.75% (e.g. from 670 to 665) can lead to failure of spontaneous seizure termination (Figure 3.7). Traveling waves reach the pathological boundaries, but, instead of being terminated, they are reflected and continue to produce seizing activity within the pathological zone. This can potentially explain the dynamical mechanisms of status epilepticus.

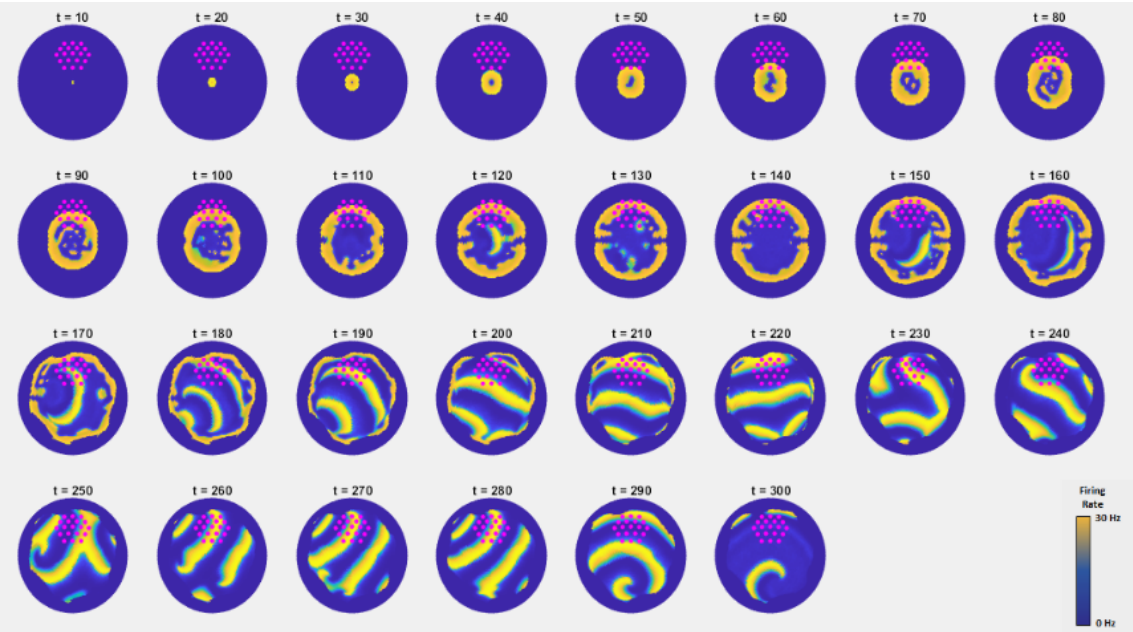

Figure 3.7: **Simulation that does not terminate spontaneously.** When the global long-range inhibition decreases, simulations occasionally do not terminate spontaneously. Traveling waves are reflected at the pathological boundaries and continue to propagate indefinitely. We hypothesize that this could be a presentation of status epilepticus.

3.2 Cortical geometry model

To achieve higher spatial resolution and increase anatomical accuracy (for both the cortical surface and the modeled electrodes), we further modified the geometry of our model by increasing the number of nodes to 40962 and warping the sphere into the geometry of a cortex. The triangular mesh of the surface is acquired through *FreeSurfer*. Electrodes are modeled by identifying a two 5x5 grids (one for macroelectrodes and one for microelectrodes) that overlay the cortical area of interest. Each electrode summarizes activity of nearby network nodes, weighted by their reciprocal distances.

In Figure 3.8, we show a simulation of a full seizure with this new model (in parallel to Figure 3.1). We can see that neural dynamics are again observed at two different times scales (less obvious here due to unseen parts of the sulci) – propagation of ictal wavefront and emergence of traveling waves. The seizure terminates spontaneously and synchronously across the entire cortex, with slowing of rhythmic activity approaching termination (Figure 3.10b). If we perform various analyses on the simulated recordings from the electrodes (Figure 3.9), we also observe similar features in human recordings. Coupling within the network increases after seizure onset, decreases during propagation and increases again approaching termination (Figure 3.10d). Direction of the traveling waves become more consistent in late stage of seizure and can occasionally undergo sudden changes (Figure 3.10c). This suggests that the spatial and temporal dynamics produced by our model are likely at the right order of magnitude compared to human data, such that, with electrodes modeled at the same scale as the real electrodes, the activity observed are quantitatively and qualitatively comparable to human recordings.

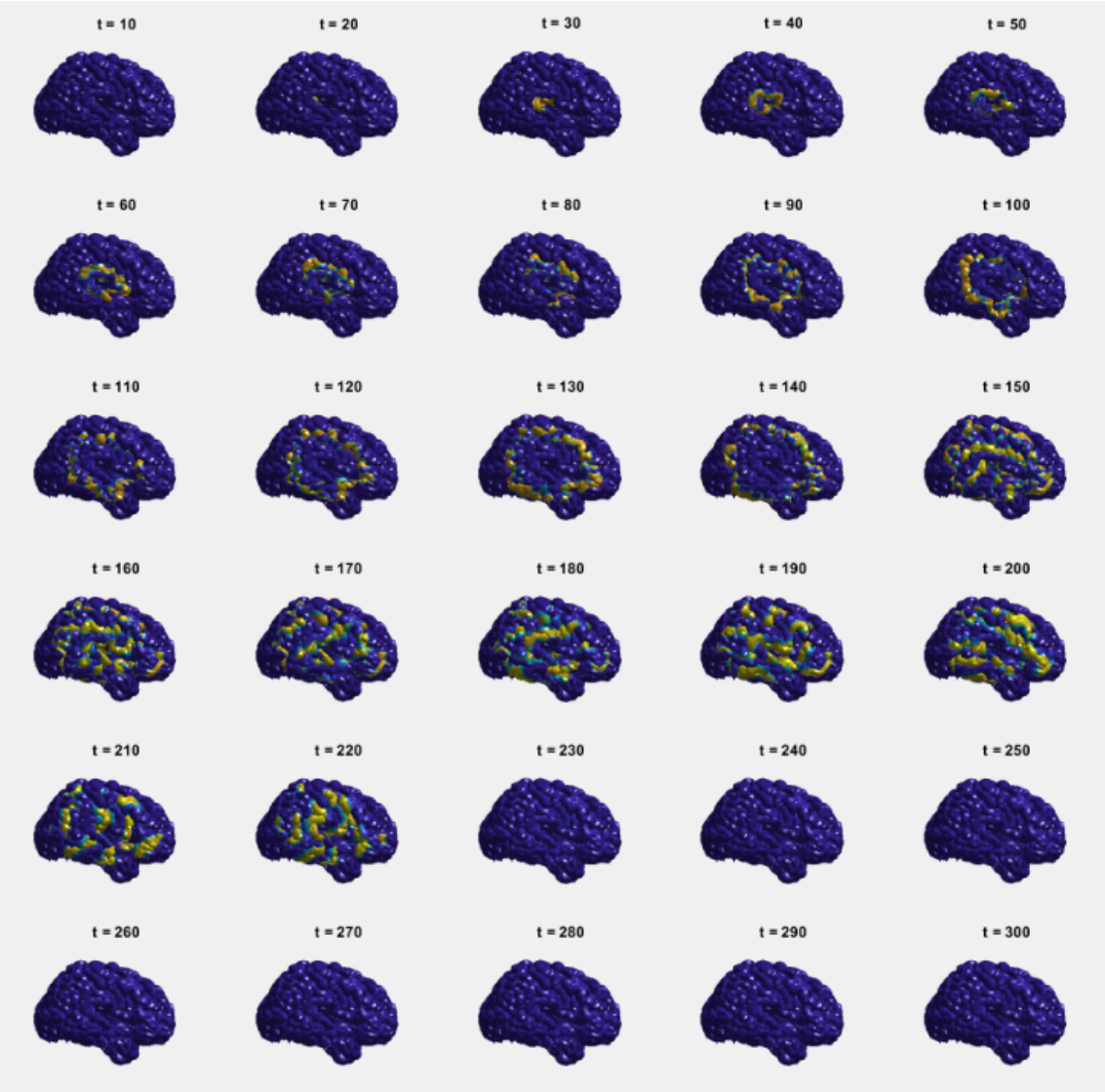

Figure 3.8: **Example spatial maps of simulated activity on the cortex.** Similar to Figure 3.1, blue areas represent quiescent populations while yellow nodes suggest high excitatory activity.

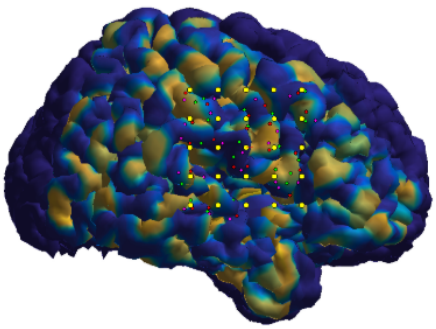

Figure 3.9: **Simulated electrodes on the cortical surface.** The yellow dots represent the simulated macroelectrodes, with size comparable to ECoG grids. The nearby green, red, pink dots are the three closest nodes on the cortical network from which the electrodes record electrical activity (as described in the text, the activity is weighted by reciprocal distances to the electrode).

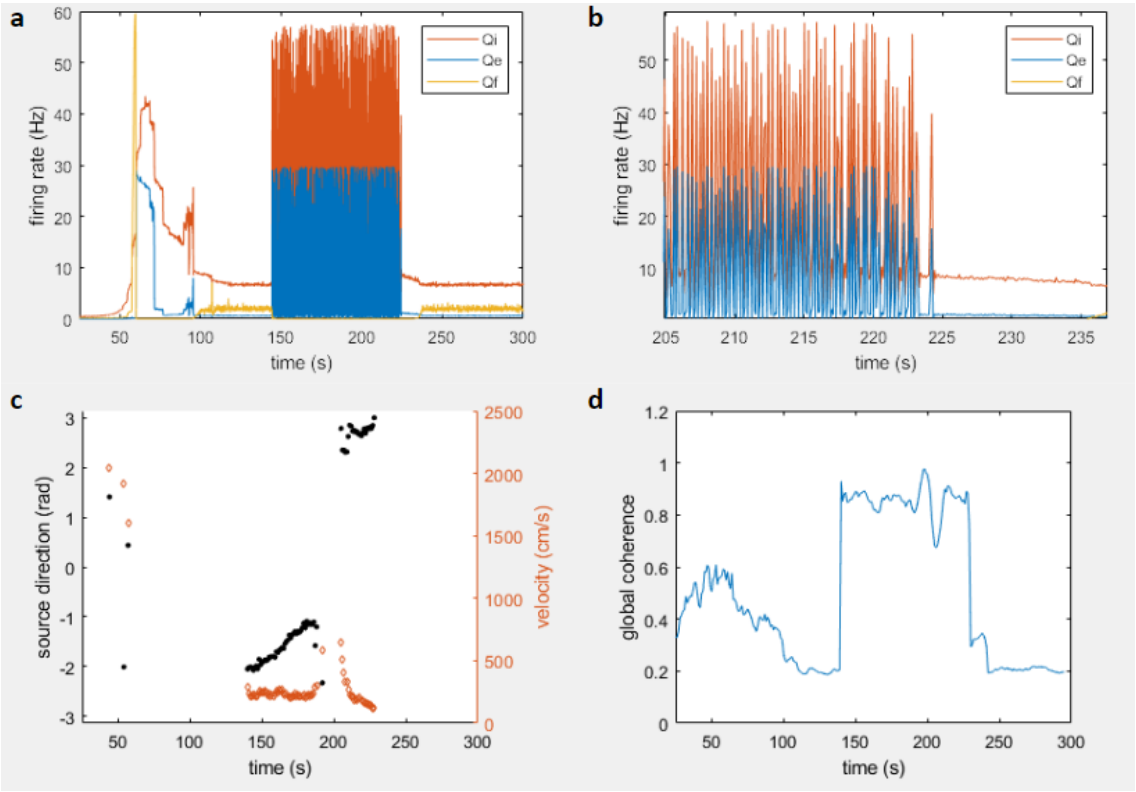

Figure 3.10: **Various analyses of the simulation from cortical geometry model.** (a) Firing rate of each neural population in entire seizure course. (b) Firing rate of each neural population prior to seizure termination. (c) Source direction and velocity recorded at the macroelectrodes throughout seizure course. (d) Global coherence at the macroelectrodes over seizure course.

3.3 Preliminary results for spontaneous ictogenesis

The majority of this work has focused on the dynamics of a focal seizure after the time of ictogenesis, i.e. the emergence of an epileptogenic focus, where seizure is initiated. Specifically, we have modeled the propagation and termination after the focus is manually incited. We recognize that modeling the process of spontaneous ictogenesis is another essential piece of puzzle in understanding the full seizure dynamics and will open many more doors towards other surgical and pharmacological interventions. We are working towards achieving this goal and we present some preliminary data in this section.

Similar to seizure termination, ictogenesis is also one of the least understood topic in epilepsy. Animal experiments have confirmed that various cellular, synaptic, network abnormalities can perturb the excitatory and inhibitory balance in the brain and lead to onset of seizure. However, the exact mechanism that governs the transition in human and why there is a sudden perturbation of balance at seizure onset are still unclear. Utilizing existing components of our model, specifically the elevated extracellular potassium, we would like to propose a possible mechanism. As discussed in Section 1.2.1, accumulation of extracellular potassium increases neural excitability and may play an important role in seizure propagation – we hypothesize that it could be the underlying mechanism for ictogenesis as well. To model this, we modify Equation 2.7 such that there is some rare, high-amplitude, temporally- and spatially-randomized excitatory current from subcortical structures into the cortex (in addition to the existing baseline subcortical input):

$$\phi^{\mathrm{sc}}_{eb}(\vec{r},t) = \langle \phi^{\mathrm{sc}}_{eb} \rangle + a\sqrt{\langle \phi^{\mathrm{sc}}_{eb} \rangle}\xi_{eb}(\vec{r},t) + b\xi'_{eb}(\vec{r},t) \tag{3.1}$$

where $\xi'_{eb}(\vec{r},t)$ is a Bernoulli function with small probability (for example, 0.0001) and b represents the amplitude of the randomized current (in this case chosen as 28). This excitation contributes to the very slow accumulation of potassium within the pathological zone, where potassium homeostasis is impaired. Within the pathological zone, there are several spot locations where potassium accumulates faster than others (e.g. representing locations where glial function is more impaired) and they gradually become slightly more excitable than surrounding areas. When one of these locations by chance also receive high-amplitude subcortical input, it may become an epileptogenic focus and initiate a seizure.

Figure 3.11 shows a simulation with this modified model. Of note, the slow accumulation of potassium is modeled at the time scale of minutes here, but can easily be adjusted to hours or days (comparable to human seizure frequency) by modifying parameters. One technical detail to note: The added high-amplitude subcortical input disrupts various spatiotemporal dynamics produced in the original model. Hence, we have had to modify the model such that the amplitude of this input (parameter b in Equation 3.1) quickly decreases when there is high cortical activity (e.g. during the ictal period). With this assumption, the spatiotemporal dynamics simulated are very similar to the original model, except that now the seizure focus arises spontaneously. All the qualitative and quantitative features that our original model is able to reproduce consistently hold true. With further exploration of parameter space, this assumption might not be necessary. However, we also wonder if this could be an alternative representation of the "Network inhibition hypothesis" proposed by Blumenfeld [50]. In its original form, this hypothesis suggests that seizures can spread from the cortex to activate inhibitory subcortical structures that in turn deactivate frontal cortex and lead to loss of consciousness. This could potentially align with our assumption that subcortical input decreases

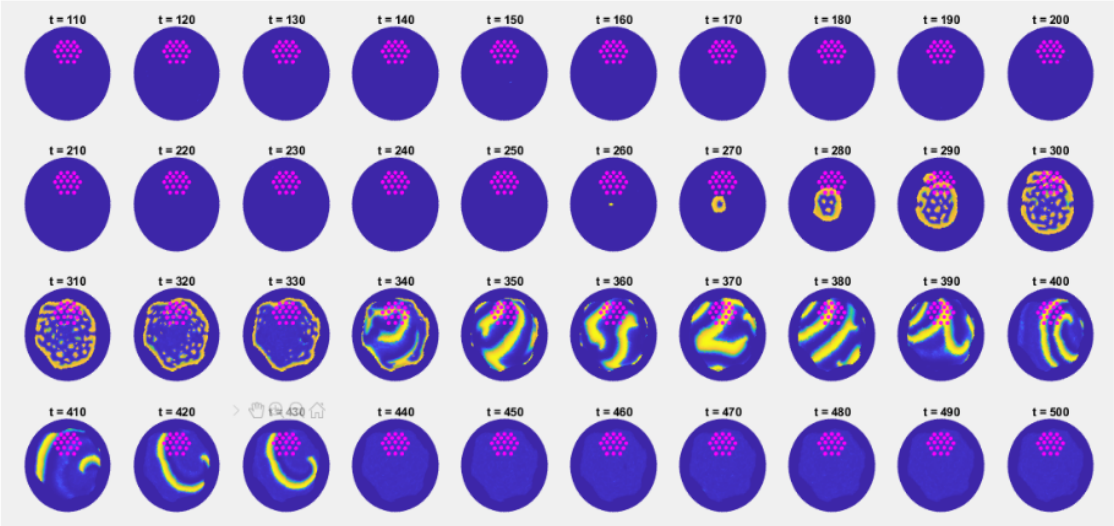

Figure 3.11: **Example spatial maps with epileptogenic focus arising from randomized subcortical input instead of manually incited.** Similar to Figure 3.1, blue areas represent quiescent populations while yellow nodes suggest high excitatory activity.

---

during the seizure.

Of note, in this model, there is already some diffuse baseline excitability (from very slow potassium accumulation) minutes prior to seizure onset. Interestingly, this matches well with some recent experimental data. Although clinically the onset of seizures is usually considered an abrupt phenomenon, there has been increasing evidence from fMRI and intracranial EEG that suggest widespread changes in cortical activity hours prior to seizure [64, 65]. Long-term monitoring with a sensitive potassium probe either in an animal model or epilepsy patient could help understand if potassium does play a role in ictogenesis.

Chapter 4

Conclusion and Discussion

Despite significant advancements in neuroscience in the past few decades, understanding and treating epilepsy remains one of the most challenging question in neurology. The brain's complexity, the disease's heterogeneous manifestation, coupled with the difficulty of performing relevant *in vivo* experiments, all hinder our ability to uncover the underlying mechanisms that sustain a seizure. Fortunately, the newest electrode technologies have enabled us to record neural activity at different spatial and temporal scales and allowed us to catch a glimpse of the assorted dynamics. As a consequence, this calls for new computational models that can explain the physiological factors underlying these observed activity. Models with different degrees of details have been proposed, all with their own strength and caveats. Some are able to portray cellular features to the level of individual ion channels and receptors, allowing investigation of how ion currents influence neural firing. Some target a wider spatial coverage and successfully reproduce the entire cortical dynamics. With current computational power, it is challenging to achieve both. Our hope is to find an appropriate middle ground, with sufficient anatomical scope to allow comparison with patients' ECoG recordings, while conserving adequate biological details to enable speculation of mechanisms.

Summary of results and discussion. In short, we developed an *in silico*, network-based, anatomically- and biophysically-motivated representation of realistic seizure activity in the human brain. We use the model in [8] as a foundation and added several elements that have been shown to play significant roles in seizure dynamics, including fast-spiking interneurons, extracellular potassium and its effect on neural excitability and depolarization block. We also increase the geometrical accuracy by expanding the grid, warping it into cortical surface, and modeling realistic electrodes that capture electrical activity. Our model reproduces several experimental findings from patient electrographic data.

Most importantly, our model consistently simulate dynamics at two distinct spatiotemporal scales – ictal wavefront and traveling waves. When seizure initiates in a small epileptogenic focus, an ictal wavefront slowly propagates outwards, recruiting neighboring areas into abnormal activity. Later in the seizure, traveling waves (spike-and-wave discharges) emerge within the recruited area and are seen in both microscopic and macroscopic electrode recordings. These waves propagate orders of magnitude faster than the ictal wavefront (100-1000 mm/s versus 1 mm/s). Various versions of our model suggest that more than one cellular mechanism can possibly govern these observations. Specifically, we confirm that breakdown of surrounding inhibitory barrier from depolarization block (as a result of extracellular potassium accumulation) can precipitate seizure recruitment, but it is certainly not necessary – hyperexcitability from potassium accumulation alone may be sufficient in overcoming the brain's normal inhibitory

barrier, though the potassium production/leakage needs to be relative fast (e.g. in cases of channelopathies). One possible experiment to differentiate between these two scenarios is to modify the ion conductance of the fast-spiking interneurons to prevent them from entering depolarization block, then observe if a seizure can be initiated in setting of high external excitatory input. There are also other possible mechanisms that our framework does not have the capability of modeling, e.g. collapsed trans-membrane chloride gradient that reduces the strength of surrounding GABA-dependent inhibition [37, 38]. Including this in our model will require entirely redesigning the properties of the nodes and edges and will likely compromise other physiologies that our model is currently able to capture. Of note, in our model, the emergence of traveling waves is dependent on slow potassium accumulation and its effect on closing gap junctions between inhibitory populations. This has been theorized in literature, though to the best of our knowledge, has not been proven with experiments [8]. Lastly, one temporal dynamics that we have not delved into much is the observed low amplitude, fast oscillations prior to transition into spike-and-wave complexes [12]. Revisiting Figure 3.2a, the excitatory activity (blue tracing) immediately after recruitment could possibly represent this fast activity. Whether this corresponds to what is recorded in human seizures and what the underlying physiology is warrant further exploration.

Contradictory studies have proposed that the source of traveling waves is either a stationary cortical source or a moving ictal wavefront [8, 40]. Our model suggests that both cases are theoretically plausible and the former happens when the focus is highly excitable and persistent. However, we would also like to point out that the two papers performed very different analyses and could be why they lead to distinct conclusions. [8] compared the directional consistency of traveling waves in human data with computational models of either scenario and concluded that the fixed cortical source is more compatible, while [40] compared the direction of the ictal wavefront against the traveling waves and suggested that the wavefront is more likely the source. In the future, it may be helpful to revisit these two analyses using our model (specifically the cortical geometry one). It is possible that only one scenario dominates, and our model's more realistic representation of the ictal wavefront along with the ability to account for the sulci and gyri can help explain why they led to different outcomes. Alternatively, there are experimental procedures that can possibly distinguish the two scenarios. For example, if the traveling wave source is a fixed cortical source, application of an external stimulus at this source midway through the seizure should disrupt the emergence of traveling waves.

Another patient electrographic finding that our model is able to reproduce is the trend of spatial coupling throughout a seizure event. Specifically, the coupling within the cortical network increases shortly after seizure onset, decreases during propagation and increases again approaching termination. We hypothesize that these are correlated with the evolution of spatial activities described earlier. At onset, ictal wavefront propagation leads to increase of coherence. As traveling waves begin to emerge, they initially fail to travel far because gap junctions unite inhibitory populations, hence coherence is low. Prior to termination, gap junction weakens in setting of potassium accumulation, and waves can travel longer distance without inhibition, supporting the observed spatial coupling. Of note, the analysis in this project focuses on coherence within the frequency spectrum 1-13Hz, as the highest coherence in human seizure data is observed within this range. Many previous coupling analysis have yielded different trends, possibly due to an alternative choice of frequency range, or differences in coupling measures [52, 53, 54, 55]. Our model, unfortunately, is not well suited to to simulate activity of higher frequency.

Lastly, in our model, seizure terminates spontaneously and synchronously and the frequency of traveling waves decreases before termination, both of which are widely recognized findings from human electrographic recordings. The mechanism underlying seizure termination is one of the least understood and least studied topics in epilepsy. We would like to contribute to the conversation by providing an alternative possibility: When the ictal wavefront approaches the normal tissue, it fails to recruit more area into seizure activity as the potassium homeostasis is intact, and thus it gradually weakens until fully ceasing. One possible experiment to study this hypothesis is to induce a global dysfunction of potassium homeostasis by selectively inhibit glial function and examine if seizure fails to terminate (in other words, always secondarily generalize).

Limitations and future directions. To the best of our knowledge, our model is the first framework that can represent seizure activity at the scale of the entire cortex. It is also the only biophysical model that unifies and explains all the above features regarding the spatiotemporal dynamics of seizures. However, several limitations should be discussed and improved in future iterations of the model. First, our current model assumes homogeneous connectivity across the entire cortex, which is a necessary simplification at this stage to ensure that the computational complexity is scalable. In the future, connectome data should be incorporated when available. It would not only help us understand how heterogeneous long-range activity influences seizure spread but will also allow us to personalize the model parameters to each patient's ECoG data and connectome data. Second, we incorporated very limited cell-level details (e.g. Goldman-Hodgkin-Katz equation, potassium efflux) to help portray the hypothesized mechanisms underlying seizure dynamics, and by necessity we have to assume some of the variables in these equations are constant. With greater computing power, the model can more realistically represent ion channels, ion concentrations and transmembrane fluxes, which will certainly increase the accuracy of the model. Nevertheless, we are hopeful that, even with the present simplifications, our model can still serve as a means to begin understanding various mechanisms underlying seizure initiation, propagation and termination.

Clinical implications. With the various hypotheses and results presented here, we would like to suggest potential medical and surgical therapies for controlling seizures. To target the mechanisms that support seizures, possible therapies include preventing potassium accumulation by restoring glial function or chelation with pharmacological measures, and preventing fast-spiking interneurons from entering depolarization block. Alternatively, from a structural perspective, our model suggests that removal or isolation of the cortical source may disrupt recruitment of tissue beyond its scope. The beauty of computational models is that these interventions can be tested *in silico* prior to designing animal models. This is certainly a future direction of our project.

The model is not only customizable to unique clinical cases, but also allows incorporation of additional biological and chemical mechanisms as they are discovered through *in vivo* and *in vitro* experiments. Ultimately, we envision continuously refining the model and contributing to personalized medicine by developing an algorithmic pipeline that tailors treatments (pharmacological, surgical and stimulation-based) in a patient-specific context, based on their clinical history, imaging data, electrographic activity and seizure subtype. We also anticipate that this framework will serve as a starting point for the computational modeling of other neurological diseases.

Bibliography

[1] Poonam Nina Banerjee, David Filippi, and W Allen Hauser. The descriptive epidemiology of epilepsy - A review. *Epilepsy Research*, 85(1):31–45, 2009.

[2] Stephan U Schuele and Hans O Lüders. Intractable epilepsy: management and therapeutic alternatives. *The Lancet Neurology*, 7(6):514–524, 2008.

[3] Fabrice Wendling, Pascal Benquet, Fabrice Bartolomei, and Viktor K Jirsa. Computational models of epileptiform activity. *Journal of Neuroscience Methods*, 260:233–251, 2016.

[4] Wulfram Gerstner and Werner M Kistler. Spiking Neuron Models: Single Neurons, Populations, Plasticity. *Book*, page 494, 2002.

[5] Hugh R Wilson and Jack D Cowan. Excitatory and Inhibitory Interactions in Localized Populations of Model Neurons. *Biophysical Journal*, 12(1):1–24, 1972.

[6] Ivan Soltesz and Kevin Staley. *Computational Neuroscience in Epilepsy*. Academic Press, 2008.

[7] Moira L Steyn-ross, D Alistair Steyn-ross, and Jamie W Sleigh. Interacting Turing-Hopf instabilities drive symmetry-breaking transitions in a mean-field model of the cortex: A mechanism for the slow oscillation. *Physical Review X*, 3(2):1–19, 2013.

[8] L E Martinet, G Fiddyment, Joseph R Madsen, Emad N Eskandar, Uri T Eden, and Sydney S Cash. Human seizures couple across spatial scales through traveling wave dynamics. *Nature Communications*, 8:1–13, 2017.

[9] Delphine Cosandier-Rimélé, Jean Michel Badier, Patrick Chauvel, and Fabrice Wendling. A physiologically plausible spatio-temporal model for EEG signals recorded with intracerebral electrodes in human partial epilepsy. *IEEE Transactions on Biomedical Engineering*, 54(3):380–388, 2007.

[10] Delphine Cosandier-Rimélé, I Merlet, J M Badier, P Chauvel, and Fabrice Wendling. The neuronal sources of EEG: Modeling of simultaneous scalp and intracerebral recordings in epilepsy. *NeuroImage*, 42(1):135–146, 2008.

[11] Viktor K Jirsa, William C Stacey, Pascale P Quilichini, Anton I Ivanov, and Christophe Bernard. On the nature of seizure dynamics. *Brain*, 137(8):2210–2230, 2014.

[12] Timothée Proix, Fabrice Bartolomei, Maxime Guye, and Viktor K Jirsa. Individual brain structure and modelling predict seizure propagation. *Brain*, 140(1):641–654, 2017.

[13] LF Abbott. Theoretical Neuroscience Rising, 2008.

[14] Zhang J. Zhang, Julius Koifman, Damian S. Shin, Hui Ye, Carlos M. Florez, Liang Zhang, Taufik A. Valiante, and Peter L. Carlen. Transition to seizure: Ictal discharge is preceded by exhausted presynaptic GABA release in the hippocampal CA3 region. *Journal of Neuroscience*, 2012.

[15] Valeri Lopantsev and Massimo Avoli. Participation of GABA(A)-mediated inhibition in ictallike discharges in the rat entorhinal cortex. *Journal of Neurophysiology*, 1998.

[16] Rüdiger Köhling, Martin Vreugdenhil, Enrico Bracci, and John G.R. Jefferys. Ictal epileptiform activity is facilitated by hippocampal GABA(A) receptor-mediated oscillations. *Journal of Neuroscience*, 2000.

[17] Mark P. Beenhakker and John R. Huguenard. Neurons that Fire Together Also Conspire Together: Is Normal Sleep Circuitry Hijacked to Generate Epilepsy?, 2009.

[18] Vadym Gnatkovsky, Laura Librizzi, Federica Trombin, and Marco De Curtis. Fast activity at seizure onset is mediated by inhibitory circuits in the entorhinal cortex in vitro. *Annals of Neurology*, 2008.

[19] L E Martinet, Omar J Ahmed, Kyle Q Lepage, Sydney S Cash, and Mark A Kramer. Slow Spatial Recruitment of Neocortex during Secondarily Generalized Seizures and Its Relation to Surgical Outcome. *Journal of Neuroscience*, 35(25):9477–9490, 2015.

[20] Catherine A. Schevon, Steven Tobochnik, Tahra Eissa, Edward Merricks, Brian Gill, R. Ryley Parrish, Lisa M. Bateman, Guy M. McKhann, Ronald G. Emerson, and Andrew J. Trevelyan. Multiscale recordings reveal the dynamic spatial structure of human seizures. *Neurobiology of Disease*, 127(January):303–311, 2019.

[21] Andrew J Trevelyan, David Sussillo, and Rafael Yuste. Feedforward inhibition contributes to the control of epileptiform propagation speed. *Journal of Neuroscience*, 27(13):3383–7, 2007.

[22] Catherine A Schevon, Shennan A Weiss, Guy M Mckhann, Robert R Goodman, Rafael Yuste, Ronald G Emerson, and Andrew J Trevelyan. Evidence of an inhibitory restraint of seizure activity in humans. *Nature communications*, 3:1060, 2012.

[23] Sattar Khoshkhoo, Daniel Vogt, Vikaas S Sohal, Sattar Khoshkhoo, Daniel Vogt, and Vikaas S Sohal. Dynamic , Cell-Type-Specific Roles for GABAergic Interneurons in a Mouse Model of Optogenetically Inducible Seizures Dynamic , Cell-Type-Specific Roles for GABAergic Interneurons in a Mouse Model of Optogenetically Inducible Seizures. *Neuron*, 93(2):291–298, 2017.

[24] Mario Cammarota, Gabriele Losi, Angela Chiavegato, Micaela Zonta, and Giorgio Carmignoto. Fast spiking interneuron control of seizure propagation in a cortical slice model of focal epilepsy. *Journal of Physiology*, 4:807–822, 2013.

[25] Michele Sessolo, Iacopo Marcon, Serena Bovetti, Gabriele Losi, Mario Cammarota, Gian Michele Ratto, Tommaso Fellin, and Giorgio Carmignoto. Parvalbumin-positive inhibitory interneurons oppose propagation but favor generation of focal epileptiform activity. *Journal of Neuroscience*, 2015.

[26] I Toyoda, S Fujita, AK Thamattoor, and PS Buckmaster. Unit Activity of Hippocampal Interneurons before Spontaneous Seizures in an Animal Model of Temporal Lobe Epilepsy. *Journal of Neuroscience*, 35(16):6600–6618, 2015.

[27] Jokubas Ziburkus, John R Cressman, Ernest Barreto, and Steven J Schiff. Interneuron and pyramidal cell interplay during in vitro seizure- like events. *Journal of Neurophysiology*, 95(6):3948–3954, 2007.

[28] Omar J Ahmed, Mark A Kramer, Wilson Truccolo, Jason S Naftulin, Nicholas S Potter, Emad N Eskandar, Garth R Cosgrove, Andrew S Blum, Leigh R Hochberg, and Sydney S Cash. Inhibitory single neuron control of seizures and epileptic traveling waves in humans. *BMC Neuroscience*, 15(JULY):F3, 2014.

[29] Damian Seung Ho Shin, Wilson Yu, Adrian Fawcett, and Peter Louis Carlen. Characterizing the persistent CA3 interneuronal spiking activity in elevated extracellular potassium in the young rat hippocampus. *Brain Research*, 1331:39–50, 2010.

[30] Fiona E N LeBeau, Stephen K Towers, Roger D Traub, Miles A Whittington, and Eberhard H Buhl. Fast network oscillations induced by potassium transients in the rat hippocampus in vitro. *The Journal of physiology*, 542(Pt 1):167–79, 2002.

[31] Leandro Leite Antonio, Marlene Lulie Anderson, Eskedar Ayele Angamo, Siegrun Gabriel, Zin Juan Klaft, Agustin Liotta, Seda Salar, Nora Sandow, and Uwe Heinemann. In vitro seizure like events and changes in ionic concentration, 2016.

[32] Allen P. Fertziger and James B. Ranck. Potassium accumulation in interstitial space during epileptiform seizures. *Experimental Neurology*, 1970.

[33] O. P. Hamill, J. R. Huguenard, and D. A. Prince. Patch-clamp studies of voltagegated currents in identified neurons of the rat cerebral cortex. *Cerebral Cortex*, 1991.

[34] Marco Martina, Jobst H. Schultz, Heimo Ehmke, Hannah Monyer, and Peter Jonas. Functional and molecular differences between voltage-gated K+ channels of fast-spiking interneurons and pyramidal neurons of rat hippocampus. *Journal of Neuroscience*, 1998.

[35] Bernardo Rudy and Chris J. McBain. Kv3 channels: Voltage-gated K+ channels designed for high-frequency repetitive firing, 2001.

[36] Ghanim Ullah, John R. Cressman, Ernest Barreto, and Steven J. Schiff. The influence of sodium and potassium dynamics on excitability, seizures, and the stability of persistent states: II. Network and glial dynamics. *Journal of Computational Neuroscience*, 2009.

[37] Junko Yamada, Akihito Okabe, Hiroki Toyoda, Werner Kilb, Heiko J. Luhmann, and Atsuo Fukuda. Cl- uptake promoting depolarizing GABA actions in immature rat neocortical neurones is mediated by NKCC1. *Journal of Physiology*, 2004.

[38] Johan Pallud, Michel Le Van Quyen, Franck Bielle, Christophe Pellegrino, Pascale Varlet, Marianne Labussiere, Noémie Cresto, Marie Joseph Dieme, Michel Baulac, Charles Duyckaerts, Nazim Kourdougli, Geneviève Chazal, Bertrand Devaux, Claudio Rivera, Richard Miles, Laurent Capelle, and Gilles Huberfeld. Cortical GABAergic excitation contributes to epileptic activities around human glioma. *Science Translational Medicine*, 2014.

[39] Hannah Alfonsa, Edward M. Merricks, Neela K. Codadu, Mark O. Cunningham, Karl Deisseroth, Claudia Racca, and Andrew J. Trevelyan. The contribution of raised intraneuronal chloride to epileptic network activity. *Journal of Neuroscience*, 2015.

[40] Elliot H Smith, Jyun-you Liou, Tyler S Davis, Edward M Merricks, Spencer S Kellis, Shennan A Weiss, Bradley Greger, Paul A House, Guy M Mckhann, Robert R Goodman, Ronald G Emerson, Lisa M Bateman, Andrew J Trevelyan, and Catherine A Schevon. The ictal wavefront is the spatiotemporal source of discharges during spontaneous human seizures. *Nature Communications*, 7:11098, 2016.

[41] Mark A Kramer, Wilson Truccolo, Uri T Eden, Kyle Q Lepage, Leigh R Hochberg, Emad N Eskandar, Joseph R Madsen, Jong W Lee, Atul Maheshwari, Eric Halgren, Catherine J Chu, and Sydney S Cash. Human seizures self-terminate across spatial scales via a critical transition. *Proceedings of the National Academy of Sciences of the United States of America*, 109(51):21116–21, 2012.

[42] Wilson Truccolo, Jacob A. Donoghue, Leigh R. Hochberg, Emad N. Eskandar, Joseph R. Madsen, William S. Anderson, Emery N. Brown, Eric Halgren, and Sydney S. Cash. Single-neuron dynamics in human focal epilepsy. *Nature Neuroscience*, 14(5):635–643, 2011.

[43] Steven J. Schiff, David Colella, Gary M. Jacyna, Elizabeth Hughes, Joseph W. Creekmore, Angela Marshall, Maribeth Bozek-Kuzmicki, George Benke, William D. Gaillard, Joan Conry, and Steven R. Weinstein. Brain chirps: Spectrographic signatures of epileptic seizures. *Clinical Neurophysiology*, 2000.

[44] K. Yamada, Juan Juan Ji, H. Yuan, T. Miki, S. Sato, N. Horimoto, T. Shimizu, S. Seino, and N. Inagaki. Protective role of ATP-sensitive potassium channels in hypoxia-induced generalized seizure. *Science*, 2001.

[45] Kevin J. Staley, Mark Longacher, Jaideep S. Bains, and Audrey Yee. Presynaptic modulation of CA3 network activity. *Nature Neuroscience*, 1998.

[46] Marom Bikson, Philip J. Hahn, John E. Fox, and John G.R. Jefferys. Depolarization block of neurons during maintenance of electrographic seizures. *Journal of Neurophysiology*, 2003.

[47] Anatol Bragin, Markku Penttonen, and György Buzsáki. Termination of epileptic afterdischarge in the hippocampus. *Journal of Neuroscience*, 1997.

[48] Adam E. Ziemann, Mikael K. Schnizler, Gregory W. Albert, Meryl A. Severson, Matthew A. Howard, Michael J. Welsh, and John A. Wemmie. Seizure termination by acidosis depends on ASIC1a. *Nature Neuroscience*, 2008.

[49] H. Blumenfeld, G. I. Varghese, M. J. Purcaro, J. E. Motelow, M. Enev, K. A. McNally, A. R. Levin, L. J. Hirsch, R. Tikofsky, I. G. Zubal, A. L. Paige, and S. S. Spencer. Cortical and subcortical networks in human secondarily generalized tonicclonic seizures. *Brain*, 2009.

[50] Hal Blumenfeld. Impaired consciousness in epilepsy, 2012.

[51] Mark A Kramer and Sydney S Cash. Epilepsy as a Disorder of Cortical Network Organization. *The Neuroscientist*, 18(4):360–372, 2012.

[52] F. Bartolomei, F. Wendling, J. Régis, M. Gavaret, M. Guye, and P. Chauvel. Pre-ictal synchronicity in limbic networks of mesial temporal lobe epilepsy. *Epilepsy Research*, 2004.

[53] F. Grenier, I. Timofeev, and M. Steriade. Focal synchronization of ripples (80-200 Hz) in neocortex and their neuronal correlates. *Journal of Neurophysiology*, 2001.

[54] Kaspar Schindler, Frédérique Amor, Heidemarie Gast, Markus Müller, Alexander Stibal, Luigi Mariani, and Christian Rummel. Peri-ictal correlation dynamics of high-frequency (80-200Hz) intracranial EEG. *Epilepsy Research*, 2010.

[55] Mark A Kramer, Uri T Eden, ED Kolaczyk, Rodrigo Zepeda, Emad N Eskandar, and Sydney S Cash. Coalescence and Fragmentation of Cortical Networks during Focal Seizures. *Journal of Neuroscience*, 30(30):10076–10085, 2010.

[56] S. C. Ponten, F. Bartolomei, and C. J. Stam. Small-world networks and epilepsy: Graph theoretical analysis of intracerebrally recorded mesial temporal lobe seizures. *Clinical Neurophysiology*, 2007.

[57] Steven J. Schiff, Tim Sauer, Rohit Kumar, and Steven L. Weinstein. Neuronal spatiotemporal pattern discrimination: The dynamical evolution of seizures. *NeuroImage*, 2005.

[58] Kaspar Schindler, Howan Leung, Christian E Elger, and Klaus Lehnertz. Assessing seizure dynamics by analysing the correlation structure of multichannel intracranial EEG. *Brain*, 130(1):65–77, 2007.

[59] Kaspar Schindler, Christian E. Elger, and Klaus Lehnertz. Increasing synchronization may promote seizure termination: Evidence from status epilepticus. *Clinical Neurophysiology*, 2007.

[60] Michael V.L. Bennett and R. Suzanne Zukin. Electrical Coupling and Neuronal Synchronization in the Mammalian Brain, 2004.

[61] Uwe Heinemann and Hans Dieter Lux. Ceiling of stimulus induced rises in extracellular potassium concentration in the cerebral cortex of cat. *Brain Research*, 1977.

[62] Jean Gotman. Measurement of small time differences between EEG channels: Method and application to epileptic seizure propagation. *Electroencephalography and Clinical Neurophysiology*, 1983.

[63] Andrew J. Trevelyan, Torsten Baldeweg, Wim Van Drongelen, Rafael Yuste, and Miles Whittington. The source of afterdischarge activity in neocortical tonic-clonic epilepsy. *Journal of Neuroscience*, 2007.

[64] Brian Litt, Rosana Esteller, Javier Echauz, Maryann D'Alessandro, Rachel Shor, Thomas Henry, Page Pennell, Charles Epstein, Roy Bakay, Marc Dichter, and George Vachtsevanos. Epileptic seizures may begin hours in advance of clinical onset: A report of five patients, 2001.

[65] Paolo Federico, David F. Abbott, Regula S. Briellmann, A. Simon Harvey, and Graeme D. Jackson. Functional MRI of the pre-ictal state. *Brain*, 2005.